

DARK SOLITONS, DISPERSIVE SHOCK WAVES, AND TRANSVERSE INSTABILITIES*

M. A. HOEFER[†] AND B. ILAN[‡]

Abstract. The nature of transverse instabilities of dark solitons for the (2+1)-dimensional defocusing nonlinear Schrödinger/Gross–Pitaevskii (NLS/GP) equation is considered. Special attention is given to the small (shallow) amplitude regime, which limits to the Kadomtsev–Petviashvili (KP) equation. We study analytically and numerically the eigenvalues of the linearized NLS/GP equation. The dispersion relation for shallow solitons is obtained asymptotically beyond the KP limit. This yields (1) the maximal growth rate and associated wavenumber of unstable perturbations and (2) the separatrix between convective and absolute instabilities. The instability properties of the dark soliton are directly related to those of oblique dispersive shock wave (DSW) solutions. Stationary and nonstationary oblique DSWs are constructed analytically and investigated numerically by direct simulations of the NLS/GP equation. It is found that stationary and nonstationary oblique DSWs have the same jump conditions in the shallow and hypersonic regimes. These results have application to controlling nonlinear waves in dispersive media.

Key words. semiclassical regime, traveling waves, vortices, Bose–Einstein condensates, nonlinear topics

AMS subject classifications. 35Q55, 35Q53, 35L67, 35C08, 37K40

DOI. 10.1137/110834822

1. Introduction. The instability of one-dimensional structures to weak, long wavelength, transverse perturbations plays an important role in multidimensional nonlinear wave propagation. Physical examples appear in nonlinear optics [1], Bose–Einstein condensates (BECs) [2], and water waves [3, 4]. Early theoretical work on the transverse instability of solitons for the Kadomtsev–Petviashvili (KP) equation [5, 6] and the nonlinear Schrödinger (NLS) equation [7, 8] focused on the existence of a linear instability and the maximal growth rate, both of which are properties of the *imaginary* portion of the spectrum of unstable modes. On the other hand, recent two-dimensional numerical simulations of NLS [9] and vector NLS [10] supersonic flows past an obstacle in two dimensions reveal the excitation of apparently stable, oblique spatial dark solitons for certain flow parameters. The resolution of this paradox, i.e., that dark NLS solitons are unstable to transverse perturbations yet can arise as stable structures in supersonic flows was explained in [11], where the instability was shown to be of *convective* type, so that transverse perturbations are carried away by the flow parallel to the soliton plane, effectively stabilizing the soliton near the obstacle. The characterization of convective versus absolute instability requires knowledge of the spectrum for a range of wavenumbers in the complex plane [12, 13]. For NLS dark solitons, the criteria can be simplified and involve the *real* (stable) portion of the spectrum [11].

One of the hallmarks of supersonic flows is the formation of shock waves. In classical viscous fluids, shock dynamics can be well understood mathematically in the context of a dissipative regularization of conservation laws (cf. [14]). However, there are fluids with negligible dissipation, whose dominant shock regularizing mechanism

*Received by the editors May 23, 2011; accepted for publication (in revised form) December 9, 2011; published electronically April 12, 2012.

<http://www.siam.org/journals/mms/10-2/83482.html>

[†]Department of Mathematics, North Carolina State University, Raleigh, NC 27695 (mahoefer@ncsu.edu).

[‡]School of Natural Sciences, University of California, Merced, CA 95343 (bilan@ucmerced.edu).

is dispersion (see the review [15]). Notably, superfluidic BECs in the repulsive regime and laser beams in optically defocusing media fall within this class of dispersive fluids. When a dispersive fluid flows at supersonic speed, it can form a dispersive shock wave (DSW) that possesses an expanding, oscillatory wavetrain with a large-amplitude, soliton edge, and small-amplitude sound wave edge. DSWs appear as special, asymptotic solutions of nonlinear dispersive equations and have been observed in BEC [16, 17, 18] and nonlinear optics [19, 20]. Their theory is much less developed than their classical (dissipative) counterparts. In particular, there has been limited study of DSW stability. Recent works numerically observe transverse instabilities for NLS DSWs resulting from dark pulse propagation on a background in two spatial dimensions [21] and for oblique DSWs in supersonic flow past a corner [22]. In the former case, the transverse instability was mitigated by introducing nonlocal nonlinearity, while in the latter case, the convective nature of the instability effectively stabilizes the oblique DSW in certain parameter regimes. In contrast, oblique shock waves in multidimensional, classical gas dynamics are known to be linearly stable when the downstream flow is supersonic [23, 24, 25]. (See also the review article [26] for more general results.)

The aim of this work is to clarify the role of absolute and convective instabilities as they relate to spatial dark solitons and apply this understanding to oblique DSWs. Analytical and computational challenges include

- the multidimensional nature of the flows;
- the general criteria for absolute and convective instabilities requires detailed knowledge of the spectrum;
- long time integration and large spatial domains are required to properly resolve DSWs numerically.

To address these challenges, we *asymptotically* determine the spectrum of transverse perturbations to shallow but finite amplitude NLS dark solitons beyond the KP limit. This enables determination of the maximal growth rate and associated wavenumber of unstable perturbations as functions of the soliton amplitude. In addition, using adjoint methods, we introduce a simple, accurate method for *computing the spectrum and its derivatives* numerically for arbitrary soliton amplitudes. *Simplified criteria* for the determination of the *separatrix* between absolute and convective instabilities are derived. The separatrix is determined in terms of the critical Mach number M_{cr} as it relates to the soliton far field flow. Oblique dark solitons are convectively unstable when $M \geq M_{\text{cr}}$ and absolutely unstable otherwise. Using the shallow soliton asymptotics and numerical computations of the spectrum, we determine M_{cr} , demonstrating that $1 < M_{\text{cr}} \lesssim 1.4374$ with M_{cr} monotonically increasing with the soliton amplitude.

The oblique DSW trailing edge is well approximated by an oblique dark soliton. In this study, we apply the soliton stability results to the oblique DSW trailing edge in the stationary and nonstationary cases. Stationary oblique DSWs result from the solution of a boundary value problem (supersonic corner flow), while the nonstationary case arises in the solution of a Riemann initial value problem. We find that oblique DSWs with supersonic downstream flows can be absolutely unstable in contrast to classical oblique shocks. We also show that stationary and nonstationary oblique DSWs have the same downstream flow properties in the shallow and hypersonic regimes.

We consider the (2+1)-dimensional defocusing nonlinear Schrödinger/Gross-Pitaevskii (NLS/GP) equation

$$(1.1) \quad i\psi_t = -\frac{1}{2}(\psi_{xx} + \psi_{yy}) + |\psi|^2\psi, \quad (x, y) \in \mathbb{R}^2, \quad t > 0,$$

along with appropriate initial or boundary data. Equation (1.1) models matter waves in repulsive BECs and intense laser propagation in optically defocusing (i.e., with normal dispersion) media. In the variables

$$(1.2) \quad \psi = \sqrt{\rho} e^{i\phi}, \quad (u, v) = \nabla \phi,$$

(1.1) can be recast in terms of fluid-like variables, i.e., density ρ and superfluid velocity (u, v) , as

$$(1.3a) \quad \rho_t + (\rho u)_x + (\rho v)_y = 0,$$

$$(1.3b) \quad u_t + uu_x + vu_y + \rho_x = \frac{1}{4} \left(\frac{\rho_{xx} + \rho_{yy}}{\rho} - \frac{\rho_x^2 + \rho_y^2}{2\rho^2} \right)_x,$$

$$(1.3c) \quad v_t + uv_x + vv_y + \rho_y = \frac{1}{4} \left(\frac{\rho_{xx} + \rho_{yy}}{\rho} - \frac{\rho_x^2 + \rho_y^2}{2\rho^2} \right)_y.$$

Note that (1.3) in the dispersionless regime (neglecting the right-hand sides) correspond to the classical shallow water equations (Euler equations of gas dynamics with adiabatic constant $\gamma = 2$) with the speed of sound $\sqrt{\rho}$ [27].

The outline of this paper is as follows. Section 2 discusses the spectrum of unstable transverse perturbations of dark solitons with asymptotic resolution of the maximal growth rate and associated wavenumber in the shallow regime. In section 3, we recap the general criteria for absolute and convective instabilities and then carefully derive simplified criteria for oblique dark solitons. The separatrix M_{cr} is then determined. In section 4, we construct nonstationary oblique DSWs of arbitrary amplitude and stationary oblique DSWs in the shallow regime, showing the connection between their downstream flows. The stationary case is compared with (2+1)-dimensional numerical simulations. Convective and absolute instabilities of oblique DSWs are determined using the separatrix for the trailing edge dark soliton. Our numerical methods are presented in section 5. Finally, section 6 contains a discussion of the results and the applicability of our methods to other nonlinear dispersive problems.

2. Transverse instability of dark solitons. It is well known that dark soliton solutions of (1.1) exhibit an instability to perturbations of sufficiently long wavelength in the transverse direction along the soliton plane [8]. The eigenvalue problem associated with linearizing (1.1) about the dark soliton leads to the dispersion relation for unstable perturbations. Beyond demonstrating the *existence* of an instability, knowledge of the dispersion relation for a range of wavenumbers yields important *properties* of the instability, such as the growth rate Γ_{max} , the maximally unstable wavenumber k_{max} , and whether the instability is convective or absolute.

An example numerical computation of the eigenvalues for the spectral problem in (2.7) is shown in Figure 2.1. Since exact expressions are not known, asymptotic approaches leveraging the shallow dark soliton, KP limit [6, 28], and others [29, 11] have been devised. In this section, we complement these results by determining the next order correction to the dispersion relation for shallow dark solitons resulting in accurate approximation across a wider range of soliton amplitudes. We use this to determine Γ_{max} and k_{max} asymptotically. These calculations are verified numerically.

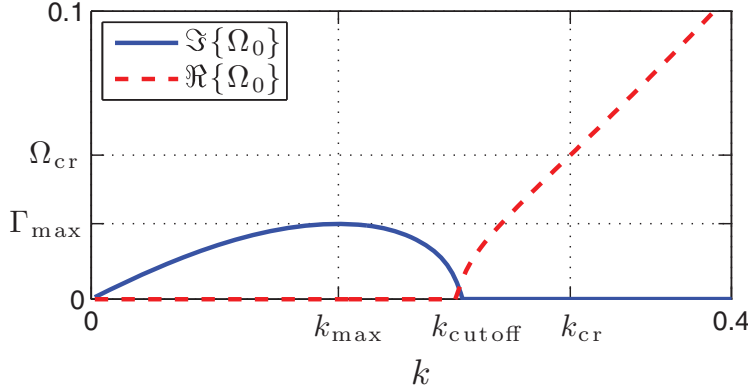


FIG. 2.1. Numerically computed real (dashes) and imaginary (solid) parts of the discrete eigenvalue $\Omega_0(k; \nu)$ of the linearized NLS equation (spectral problem (2.7)) as functions of k for $\nu = 0.5$. Delineated on the axes are (i) the cutoff wavenumber k_{cutoff} (2.11), where the eigenvalue transitions from purely imaginary to real, (ii) the maximal growth wavenumber and growth rate $(k_{\text{max}}, \Gamma_{\text{max}})$ (2.14), and (iii) the critical wavenumber and associated eigenvalue $(k_{\text{cr}}, \Omega_{\text{cr}})$ (3.8) corresponding to the transition between absolute/convective instabilities.

2.1. Dark soliton. Up to spatiotemporal shifts and an overall phase, the most general line dark soliton solution of (1.1) is

(2.1)

$$\begin{aligned} \psi'_s(x', y', t') &= \sqrt{\rho} \{ \cos \phi + i \sin \phi \tanh [a(\sin \beta x' - \cos \beta y' - vt')] \} \\ &\quad \times \exp \left\{ i \left[cx' + dy' - \left(\frac{c^2 + d^2}{2} + \rho \right) t' \right] \right\}, \\ a &= \sqrt{\rho} \sin \phi, \quad v = c \sin \beta - d \cos \beta - \sqrt{\rho} \cos \phi, \quad \phi \in [0, \pi], \quad \beta \in (0, \pi], \end{aligned}$$

where ρ is the background density and 2ϕ is the phase variation across the soliton, which together determine the depression amplitude as $\sqrt{\rho} |\sin \phi|$. The soliton is propagating at an angle β with respect to the (horizontal) x' axis with horizontal and vertical flow velocities c and d , respectively. Interpreting this solution in the fluid context with density $|\psi'_s|^2$ and flow velocity $\nabla \arg \psi'_s$, the soliton is a localized density depression on a uniformly flowing background. The Mach number of the background flow is the total flow velocity divided by the speed of sound

$$(2.2) \quad M = \sqrt{\frac{c^2 + d^2}{\rho}}.$$

The soliton has the far field behavior

$$\begin{aligned} \sin \beta x' - \cos \beta y' &\rightarrow \pm \infty, \\ \psi'_s(x', y', t') &\rightarrow \sqrt{\rho} \exp \left\{ \pm i \phi + i \left[cx' + dy' - \left(\frac{c^2 + d^2}{2} + \rho \right) t' \right] \right\}. \end{aligned}$$

Thus, five parameters determine the soliton uniquely, i.e., ρ, ϕ, β, c, d .

Using the invariances of (1.1) associated with rotation, Galilean transformation, scaling, and phase, we apply the coordinate transformation

$$(2.3) \quad \begin{aligned} \psi_s(x, y, t) = & \frac{-i}{\sqrt{\rho}} e^{-i \left[(c \sin \beta - d \cos \beta) \frac{x}{\sqrt{\rho}} + (c \cos \beta + d \sin \beta) \frac{y}{\sqrt{\rho}} + \frac{(c^2 + d^2)t}{2\rho} \right]} \\ & \times \psi'_s \left(\frac{1}{\sqrt{\rho}} (\sin \beta x + \cos \beta y) + \frac{c}{\rho} t, \frac{1}{\sqrt{\rho}} (-\cos \beta x + \sin \beta y) + \frac{d}{\rho} t, \frac{t}{\rho} \right), \end{aligned}$$

leading to the one-parameter family of dark solitons

$$(2.4) \quad \psi_s(\xi, y, t) = [i\kappa + \nu \tanh(\nu\xi)] e^{-it}, \quad \nu^2 + \kappa^2 = 1,$$

(after dropping the prime from ψ'_s) where $\nu = |\sin \phi| \in (0, 1]$ and the frame moving with the soliton is

$$\xi \doteq x - \kappa t.$$

The soliton amplitude is ν . When $\nu \ll 1$ the dark soliton is in the shallow amplitude regime. The soliton speed is $\kappa = -\cos \phi = \sqrt{1 - \nu^2}$.

2.2. Linearized eigenvalue problem. To study the transverse instabilities of the dark soliton (2.4), we consider the ansatz for (1.1)

$$\psi(\xi, y, t) = [\psi_s(\xi, y, t)e^{it} + \varphi_R(\xi, y, t) + i\varphi_I(\xi, y, t)] e^{-it},$$

where φ_R, φ_I are the real and imaginary parts of a small perturbation to a line soliton aligned with the y axis. Linearizing (1.1) results in the system

$$(2.5) \quad \begin{aligned} \frac{\partial}{\partial t} \varphi &= \mathcal{L} \varphi, \\ \varphi &\doteq \begin{bmatrix} \varphi_R \\ \varphi_I \end{bmatrix}, \\ \mathcal{L} &\doteq \begin{bmatrix} \kappa \partial_\xi + 2\nu\kappa \tanh(\nu\xi) & -\frac{1}{2}(\partial_{\xi\xi} + \partial_{yy}) - \nu^2[2 + \operatorname{sech}^2(\nu\xi)] \\ \frac{1}{2}(\partial_{\xi\xi} + \partial_{yy}) - \nu^2[2 - 3 \operatorname{sech}^2(\nu\xi)] & \kappa \partial_\xi - 2\nu\kappa \tanh(\nu\xi) \end{bmatrix}. \end{aligned}$$

It is expedient to decompose the perturbation as

$$(2.6) \quad \varphi(\xi, y, t) = \frac{1}{2\pi} \int_{\mathbb{R}} \mathbf{f}(\xi; k) e^{i[ky - \Omega(k)t]} dk, \quad \mathbf{f}(\xi; k) \doteq \begin{bmatrix} f_1(\xi; k) \\ f_2(\xi; k) \end{bmatrix}.$$

Substituting (2.6) into (2.5) yields the linearized spectral problem

$$(2.7) \quad J L \mathbf{f}(\xi; k) = -i\Omega(k) \mathbf{f}(\xi; k),$$

where

$$(2.8) \quad L \doteq L_0 + \frac{1}{2}k^2, \quad J \doteq \begin{bmatrix} 0 & 1 \\ -1 & 0 \end{bmatrix},$$

and

$$(2.9) \quad L_0 \doteq \begin{bmatrix} -\frac{1}{2}\partial_{\xi\xi} + \nu^2[2 - 3\operatorname{sech}^2(\nu\xi)] & -\kappa\partial_\xi + 2\nu\kappa \tanh(\nu\xi) \\ \kappa\partial_\xi + 2\nu\kappa \tanh(\nu\xi) & -\frac{1}{2}\partial_{\xi\xi} - \nu^2[2 + \operatorname{sech}^2(\nu\xi)] \end{bmatrix}.$$

For $k \in \mathbb{R}$, L_0 and L are self-adjoint with respect to the $L^2(\mathbb{R})$ inner product

$$(2.10) \quad \langle \mathbf{g}, \mathbf{h} \rangle \doteq \int_{\mathbb{R}} \mathbf{g}^T \mathbf{h}^* d\xi.$$

For small k it was shown formally in [8] that (i) a double eigenvalue $\Omega(0) = 0$ bifurcates into two distinct branches with each in $i\mathbb{R}$ and (ii) there is another zero eigenvalue at the cutoff wavenumber

$$(2.11) \quad k_{\text{cutoff}} \doteq \sqrt{\nu^2 - 2 + 2\sqrt{\nu^4 - \nu^2 + 1}}, \quad \Omega(k_{\text{cutoff}}) = 0.$$

These calculations were made rigorous in [30] and can be summarized as follows.

THEOREM 2.1 (Rousset and Tzvetkov [30]). *For $k \in (-k_{\text{cutoff}}, k_{\text{cutoff}}) \setminus \{0\}$, the system (2.7) has exactly two purely imaginary eigenvalues which are simple and come in pairs $\pm\Omega_0(k)$. Therefore, the dark soliton is unstable to sufficiently long wavelength transverse perturbations. Furthermore, for $k \in \mathbb{R}$, $|k| > k_{\text{cutoff}}$, the spectrum $\Omega(k)$ is real.*

For the study of convective/absolute instabilities, knowledge of the stable portion of the spectrum when $|k| > k_{\text{cutoff}}$ is required. Based on our asymptotics and numerical computations we conjecture the following.

CONJECTURE 2.2. *For $|k| > k_{\text{cutoff}}$, there exist exactly two real, simple eigenvalues $\pm\Omega_0(k)$.*

This conjecture is a natural extension of Theorem 2.1 to the real portion of the spectrum. See Appendix B for further details and comments.

Without loss of generality, we choose $\Omega_0(k)$ such that $\Im\{\Omega_0(k)\} > 0$ for $0 < k < k_{\text{cutoff}}$ and $\Re\{\Omega_0(k)\} > 0$ for $k > k_{\text{cutoff}}$. Thus, $\Omega_0(k)$ is the *dispersion relation* for transverse perturbations of the dark soliton (2.4). By a suitable choice of a branch cut, the eigenvalue $\Omega_0(k)$ can be analytically continued for $k \in \mathbb{C} \setminus \{0, \pm k_{\text{cutoff}}\}$ with 0 and $\pm k_{\text{cutoff}}$ square root branch points. We denote the growth rate as

$$(2.12) \quad \Gamma(k) \doteq \Im\{\Omega_0(k)\}$$

and the eigenfunction associated with $\Omega_0(k)$ as

$$\mathbf{f}_0(\xi; k) = \begin{bmatrix} f_{0,1}(\xi; k) \\ f_{0,2}(\xi; k) \end{bmatrix}.$$

In section 5 we discuss our numerical method for computing $\Omega_0(k)$ for $k \in \mathbb{C}$. To illustrate the spectrum, Figure 2.1 shows the (real or imaginary) computed eigenvalue, $\Omega_0(k)$, and the corresponding eigenfunctions. Note that the eigenfunctions are neither symmetric nor antisymmetric. Figures 2.2 and 2.3 present the computed continuous and discrete spectra for particular wavenumbers $0 < k < k_{\text{cutoff}}$ ($\Omega_0 \in i\mathbb{R}$) and $k > k_{\text{cutoff}}$ ($\Omega_0 \in \mathbb{R}$) as well as the associated localized eigenfunctions.

2.3. Asymptotic eigenvalue. It follows from (2.11) that for shallow amplitude solitons, $0 < \nu \ll 1$, the cutoff wavenumber is small, i.e., $k_{\text{cutoff}} \sim \frac{\sqrt{3}}{2}\nu^2$. In Appendix A we prove the following.

PROPOSITION 2.3. *For shallow amplitude, $0 < \nu \ll 1$, and either $k < k_{\text{cutoff}}$ or $k_{\text{cutoff}} < k \sim \mathcal{O}(\nu^2) \ll 1$, the eigenvalue for (2.7) formally satisfies*

$$(2.13) \quad \Omega_0(k) = \underbrace{\frac{k}{3}\sqrt{2\sqrt{3}k - 3\nu^2}}_{\text{KP}} + \underbrace{\frac{k^2(\sqrt{3}\nu^2 - k)}{6\sqrt{2\sqrt{3}k - 3\nu^2}}}_{\text{NLS correction}} + \mathcal{O}(k^{7/2}),$$

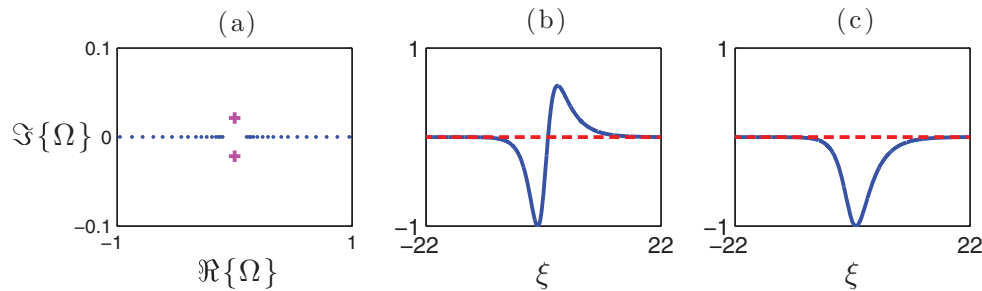


FIG. 2.2. (a) Numerical approximation of the continuous spectrum (\bullet) and the two purely imaginary discrete eigenvalues $\pm\Omega_0 \approx \pm 0.022i$ ($+$) computed for the linearized system (2.7) with $\nu = 0.5$ and $k = 0.2 < k_{\text{cutoff}} \approx 0.23$ (2.11). The real (solid) and imaginary (dashed) parts of the two component localized eigenfunctions corresponding to Ω_0 are shown in (b) $f_{0,1}(\xi)$ and (c) $f_{0,2}(\xi)$.

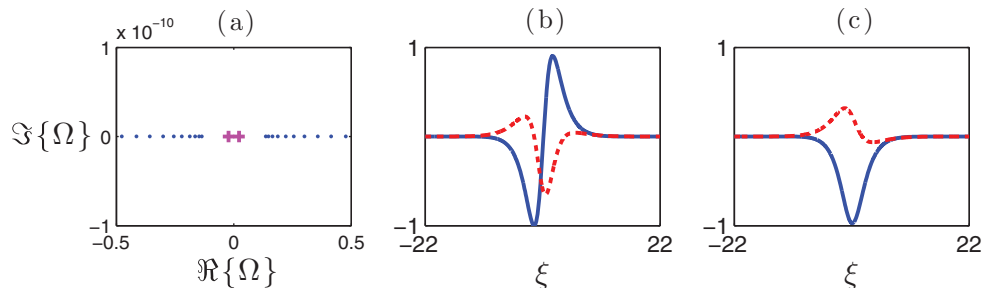


FIG. 2.3. Same as for Figure 2.2 for $k = 0.25 > k_{\text{cutoff}}$ and $\pm\Omega_0 \approx \pm 0.0215i$.

where the first (leading order) $\mathcal{O}(k^{3/2})$ term is the dispersion relation for the KP equation and the second term is the $\mathcal{O}(k^{5/2})$ correction arising from the NLS equation.

Equation (2.13) gives an asymptotic approximation to the eigenvalue for long wave perturbations of shallow dark solitons. The dispersion relation for the KP equation is well known (cf. [6, 28]). The new $\mathcal{O}(k^{5/2})$ correction term enables us to accomplish the following.

- Implement an accurate, explicit calculation of the maximal growth rate and associated wavenumber of unstable perturbations (section 2.4).
- Show that the separatrix between absolute and convective instabilities is *supersonic* (section 3.3).
- Validate the numerical computations of $\Omega_0(k)$, which are computationally demanding, especially in the shallow regime.

2.4. Calculation of the maximal growth rate. The maximal growth wavenumber k_{max} and the maximal growth rate Γ_{max} are defined by

$$(2.14) \quad \Omega'_0(k_{\text{max}}) = 0, \quad \Gamma_{\text{max}} = \Im\{\Omega_0(k_{\text{max}})\}.$$

Since $\Omega_0(k)$ is real for $k > k_{\text{cutoff}}$ it follows that $k_{\text{max}} < k_{\text{cutoff}}$ (see Figure 2.1). Using Proposition 2.3 we find the next corollary.

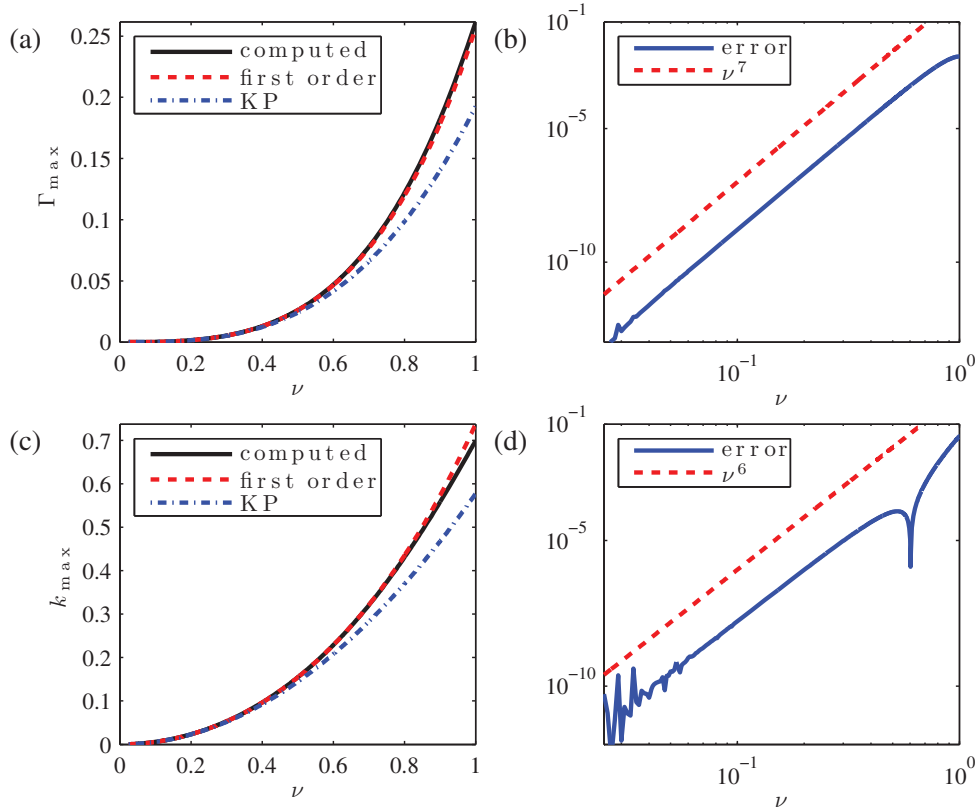


FIG. 2.4. Numerically computed maximal growth rate Γ_{\max} (a) and maximally unstable wavenumber k_{\max} (c) as functions of ν for dark solitons of the NLS equation (1.1). The KP limit and its first order correction are presented for comparison. Plots (b) and (d) are the corresponding differences between the highly accurate computed values and asymptotic approximations (2.15)–(2.16), exhibiting the expected scaling with ν .

COROLLARY 2.4.

$$(2.15) \quad k_{\max} = \underbrace{\frac{\nu^2}{\sqrt{3}}}_{\text{KP}} + \underbrace{\frac{5\nu^4}{18\sqrt{3}}}_{\text{NLS correction}} + \mathcal{O}(\nu^6),$$

$$(2.16) \quad \Gamma_{\max} = \underbrace{\frac{\nu^3}{3\sqrt{3}}}_{\text{KP}} + \underbrace{\frac{\nu^5}{9\sqrt{3}}}_{\text{NLS correction}} + \mathcal{O}(\nu^7).$$

The proof follows by expanding k_{\max} and Γ_{\max} for small ν and solving (2.14) with the approximation (2.13).

A comparison of these results with numerical computations (discussed in section 5) is shown in Figure 2.4. The computations exhibit excellent agreement with the asymptotics as well as the expected scaling of the errors with ν .

3. Convective and absolute instabilities of dark solitons. We begin by reviewing the notions of absolute/convective instabilities and the general criteria for distinguishing between them. For more detailed discussions see [12, 13, 31, 32, 33].

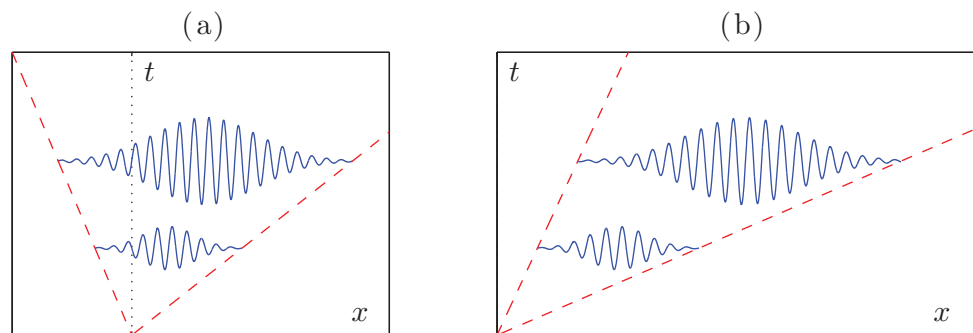


FIG. 3.1. Illustration of (a) absolutely and (b) convectively unstable waves.

Qualitatively, absolute and convective instabilities can be defined as follows (see illustration in Figure 3.1).

DEFINITION 3.1. A solution is said to be absolutely unstable if generic, small, localized perturbations grow arbitrarily large in time at each fixed point in space. A solution is said to be convectively unstable if small, localized perturbations grow arbitrarily large in time but decay to zero at any fixed point in space.

It is important to note that Definition 3.1 depends implicitly on the reference frame. This can be gleaned from Figure 3.1, where panel (b) is a rotation in the x - t plane of panel (a). Such a rotation implies that the observer in (b) is moving faster to the left than the observer in (a). Thus, if the observer “outruns” the growing perturbation, then the instability is convective. Equivalently, if the background flow speed is faster than the expanding, unstable perturbation, and after sufficient time passes the solution returns to its unperturbed state, the instability is convective. For dark solitons, the physically interesting frame of reference is the one that moves with the soliton. In this frame, the soliton is called a *spatial* dark soliton. See section 3.4.

3.1. Review of the general criteria for distinguishing between instabilities. Absolute and convective instabilities can be distinguished analytically. Consider an initial value problem on the entire line, i.e., a (1+1)-dimensional linearized system on $(x, t) \in \mathbb{R} \times (0, \infty)$. The usual approach for studying instabilities is to consider a small, spatially extended *plane wave* perturbation $e^{i(kx - \omega t)}$ of some wavenumber k and corresponding frequency $\omega = \Omega(k)$ determined by a zero of the dispersion function $\mathcal{D}(\omega, k) = 0$. The zero state is *stable* if and only if $\Im\{\Omega(k)\} \leq 0$ for all zeros of the dispersion function. However, the evolution of a particular, localized perturbation involves a Fourier integral over all real wavenumbers so that treating a single wavenumber is insufficient to fully describe any instabilities observed (or not observed) in a physical system [12].

The resolution calls for a different approach to instability analysis. Instead of a plane wave perturbation one assumes that the system is perturbed by a localized *impulse*, i.e., a Dirac delta function at position x and time $t = 0$. In this case the solution is the Green’s function

$$(3.1) \quad G(x, t) = \iint \frac{e^{i(kx - \omega t)}}{\mathcal{D}(\omega, k)} d\omega dk,$$

where the Fourier integral in k is carried out over real wavenumbers and the frequency integral (inverse Laplace transform) is performed on the Bromwich contour that lies

above all zeros of $\mathcal{D}(k, \omega)$. In connection with the plane wave analysis, the system is unstable if and only if the solution grows without bound along *some* reference frame, i.e., there is a velocity V such that for fixed x ,

$$G(x - Vt, t) \xrightarrow{t \rightarrow \infty} \infty \Leftrightarrow \text{unstable.}$$

However, when considering a *particular* reference frame, say, $\xi = x - V_0 t$ for fixed V_0 , if the solution grows without bound (resp., decays to zero) at a certain fixed point in space, x , then the system is absolutely (resp., convectively) unstable in this reference frame, i.e.,

- $G(x - V_0 t, t) \xrightarrow{t \rightarrow \infty} \infty \Leftrightarrow$ absolutely unstable,
- $G(x - V_0 t, t) \xrightarrow{t \rightarrow \infty} 0 \Leftrightarrow$ convectively unstable.

Exponential integrals of the type in (3.1) have two competing effects. Zeros of the dispersion function $\omega = \Omega(k)$ can lead to either exponential growth when $\Im\{\Omega(k)\} > 0$ or to cancellation and decay due to rapid oscillations of the integrand when $\Im\{\Omega(k)\} = 0$ for large t . To ascertain whether the system is absolutely or convectively unstable one needs to discover which of these opposite tendencies dominates. A number of methods for distinguishing between convective and absolute instabilities have been suggested, dating back to the work of Sturrock [12] and Briggs [13]. See also [34, 35, 36]. For completeness we outline the general criteria below.

It is assumed that $\mathcal{D}(\omega, k)$ is known explicitly. The ω -integral in (3.1) is along a contour that lies above all the zeros of $\mathcal{D}(\omega, k)$ for each fixed, real k and we further assume that $\mathcal{D}(\omega, k)$ is entire in (ω, k) above this contour. Hence, for $t > 0$ the ω -integral may be carried out by closing the contour in the lower half-plane and summing over the residues of the dispersion function expanded at each of its roots. Assuming the roots of $\mathcal{D}(\omega, k)$ are simple (multiple roots do not pose a serious difficulty [32]), the resulting integral can be written as

$$(3.2) \quad G(x, t) = -2\pi i \sum_{n=1}^N \int_{-\infty}^{\infty} \frac{e^{i(kx - \Omega_n(k)t)}}{\mathcal{D}'(\Omega_n(k), k)} dk,$$

where the sum is over the N zeros of the dispersion function

$$\mathcal{D}(\Omega_n(k), k) = 0, \quad \mathcal{D}'(\omega, k) \doteq \frac{\partial \mathcal{D}(\omega, k)}{\partial \omega}.$$

The problem is to determine the long time behavior of (3.2) for which the method of steepest descent is applicable (cf. [37]). It suffices to consider the point moving with speed V , $x = Vt$. Then, by suitable deformation of the real line to the steepest descent contour, the dominant contributions arise from the saddle points of the exponent satisfying

$$\frac{d}{dk} \Omega_n(k_{n,m}) = V, \quad n = 1, \dots, N, \quad m = 1, \dots, M_n,$$

allowing for multiple saddle points along each branch of the dispersion relation. Note that the zeros of \mathcal{D}' , double roots of the dispersion function, do not contribute appreciably to the integral because they cancel in the sum (3.2) [32]. Using the method of steepest descent, one recovers the dominant long time behavior

$$G(Vt, t) \sim \mathcal{O}(e^{\gamma_{\max} t} / \sqrt{t}), \quad t \rightarrow \infty,$$

where

$$\gamma_{\max}(V) \doteq \max_{n,m} \Im \{ \Omega_n(k_{n,m}) - V k_{n,m} \}.$$

Thus, if $\gamma_{\max} > 0$, then an impulse perturbation at $t = 0$, $x = 0$ grows without bound along the line $x = Vt$ and the instability is absolute. Otherwise, if $\gamma_{\max} \leq 0$, the perturbation decays along the line $x = Vt$ and so the instability is convective. These have been referred to as the *Bers-Briggs criteria* [13, 32].

3.2. Simplified criteria for the separatrix of soliton instabilities. Many previous studies applied the general criteria for classifying instabilities to dissipative systems (plasma physics, viscous fluids, etc.) where the dispersion relation was known explicitly. Given explicit and sufficiently simple dispersion relations, the analysis of the stationary points can be carried out directly. However, the dispersion relation $\Omega(k)$ is unknown for dark solitons of the NLS equation. While $\Omega(k)$ can be computed numerically for any $k \in \mathbb{C}$, doing so would make the analysis of saddle points in the complex- k or complex- ω planes quite challenging. Fortunately, as derived below, there are simplified analytic criteria for the transition point between absolute and convective instabilities of NLS solitons that rely solely on computations of the dispersion relation for real k .

Using the Laplace transform in (2.5), the linearized evolution of an initial $L^2(\mathbb{R}^2; \mathbb{R}^2)$ perturbation $\varphi_0(\xi, y)$ to the dark soliton satisfies

$$\varphi(\xi, y, t) = \frac{1}{2\pi} \int_{C_B} e^{-i\omega t} (\mathcal{L} + i\omega)^{-1} \varphi_0(\xi, y) d\omega,$$

where the Bromwich contour C_B lies above all L^2 eigenvalues of \mathcal{L} . In order to investigate the unstable *transverse* dynamics in (y, t) , we project onto the eigenfunction \mathbf{f}_0 and perform the contour integration over C_B resulting in the following representation of the dynamics:

$$\varphi(\xi, y, t) = \frac{-i}{2\pi} \int_0^\infty \frac{e^{i(ky - \Omega_0(k)t)}}{\Omega_0(k)} \mathbf{f}_0(\xi; k) dk.$$

The integral is taken over $(0, \infty)$ by use of the invariance $k \rightarrow -k$ of the eigenpair $(\Omega_0(k), \mathbf{f}_0(\xi; k))$.

By performing a Galilean shift in the NLS (1.1) as

$$(3.3) \quad \psi(x, y, t) \rightarrow \psi'(x, y, t) = e^{i(-wy - w^2 t/2)} \psi(x, y + wt, t),$$

the dispersion relation for transverse perturbations becomes

$$(3.4) \quad \Omega_0(k) \rightarrow \Omega(k) = -wk + \Omega_0(k),$$

where $-w$ is the flow speed parallel to the plane of the dark soliton (2.4). This is equivalent to investigating the behavior of the perturbation in (3.3) along the line $y = wt$. With this substitution, we consider (3.3), whose long time asymptotic behavior requires the evaluation of

$$(3.5) \quad I(t) = \int_0^{k_{\text{cutoff}}} \frac{e^{-i\Omega(k)t}}{\Omega_0(k)} \mathbf{f}_0(k) dk, \quad t \gg 1,$$

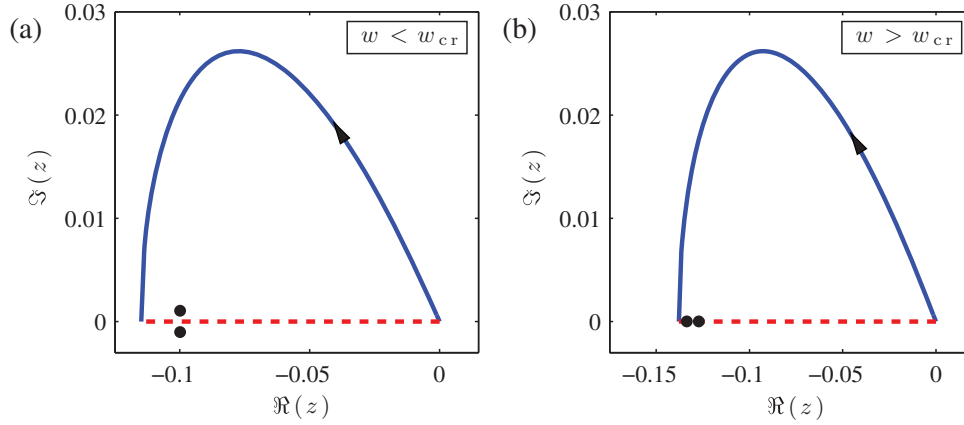


FIG. 3.2. Integration contours C (solid curves) in the complex z plane for (3.6) and the real interval $[-wk_{\text{cutoff}}, 0]$ (dashed lines). The filled circles correspond to poles of the integrand where $\Omega'(k) = \Omega'_0(k) - w = 0$, $z = \Omega(k)$, which in (a) prevent the smooth deformation of C to $[-wk_{\text{cutoff}}, 0]$ giving rise to an absolute instability. Parameter values are $\nu = 0.5$, $w_{\text{cr}} \approx 0.535$. (a) $w = 0.5 < w_{\text{cr}}$, (b) $w = 0.6 > w_{\text{cr}}$. See also Figure 3.3.

where the dependence on ξ is suppressed. The integral over $(k_{\text{cutoff}}, \infty)$ is negligible because the dispersion relation is purely real. (The stationary phase method yields algebraic decay in t ; cf. [37].) Introducing the change to a complex variable $z = \Omega(k)$, (3.5) becomes

$$(3.6) \quad I(t) = \int_C \frac{e^{-izt}}{\Omega_0(z)\Omega'(z)} \mathbf{f}_0(z) dz,$$

where $\Omega'(z) = -w + \Omega'_0(z)$ and the contour is $C \doteq \{z = \Omega(k) \mid k \in [0, k_{\text{cutoff}}]\}$. Two distinct possibilities arise:

1. A zero of Ω' gives a residue contribution to Cauchy's theorem when deforming C to the real interval $[-wk_{\text{cutoff}}, 0]$ as in Figure 3.2(a). In this case the integral diverges exponentially as $t \rightarrow \infty$ and the instability is *absolute*.
2. The zeros of Ω' do not lie between C and the real line as in Figure 3.2(b) (they may lie *on* the real axis) so that there is a smooth deformation of the contour C to the real interval $[-wk_{\text{cutoff}}, 0]$. In this case the integral decays to zero as $t \rightarrow \infty$ and the instability is *convective*.

As discussed in the previous section, the saddle points $\Omega'(k_0) = \Omega'_0(k_0) - w = 0$ give the long time asymptotic behavior $\varphi \sim \mathcal{O}(e^{i\Omega(k_0)t}/\sqrt{t})$, $t \rightarrow \infty$. As the transverse flow speed w is varied, the type of instability changes from absolute to convective. The transition from absolute to convective instability occurs at $w = w_{\text{cr}}$ when two zeros of $\Omega'(k)$ merge on the real line. That is, they form a double zero so that $\Omega''(k_{\text{cr}}) = \Omega''_0(k_{\text{cr}}) = 0$ and $\Omega'_0(k_{\text{cr}})$ is minimum. This behavior is depicted in Figures 3.2 and 3.3 with Figure 3.2(a) showing two complex conjugate zeros for $w < w_{\text{cr}}$, while Figure 3.2(b) reveals their splitting into two real zeros for $w > w_{\text{cr}}$. These real zeros are depicted in Figure 3.3 for $w > w_{\text{cr}}$. By an appropriate choice of the branch cut, one can show that $\Omega_0(k) = \Omega_0^*(k^*)$ so that complex zeros of $\Omega'(k) = \Omega'_0(k) - w$ come in conjugate pairs. This proves the next proposition.

PROPOSITION 3.2. *The critical wavenumber k_{cr} and critical transverse velocity w_{cr} for the transition between absolute and convective instability are real. They satisfy*

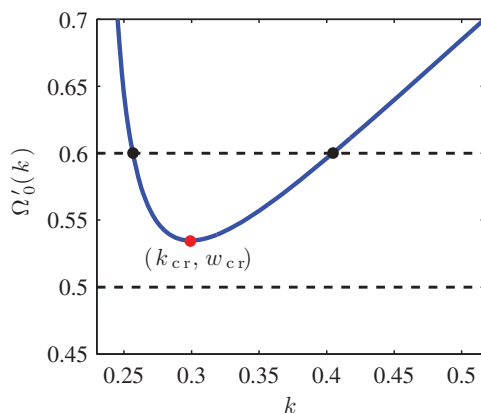


FIG. 3.3. Plot of $\Omega'_0(k)$ for real $k > k_{\text{cutoff}} \approx 0.230$ and $\nu = 0.5$. The minimum of this curve corresponds to the coalescence of the poles in Figure 3.2 and the critical transverse flow speed w_{cr} at which the instability changes from absolute to convective. The dashed lines correspond to the values of w used to compute Figure 3.2(a) (lower, absolute instability) and Figure 3.2(b) (upper, convective instability).

the simplified criteria

$$(3.7a) \quad \frac{\partial^2 \Omega}{\partial k^2}(k_{cr}; w_{cr}) = 0,$$

$$(3.7b) \quad \frac{\partial \Omega}{\partial k}(k_{cr}; w_{cr}) = 0.$$

These conditions appeared in [11].

COROLLARY 3.3.

$$(3.8a) \quad \frac{\partial^2 \Omega_0}{\partial k^2}(k_{cr}) = 0,$$

$$(3.8b) \quad w_{cr} = \frac{\partial \Omega_0}{\partial k}(k_{cr}).$$

The proof follows from (3.4) and (3.7).

When the transverse flow speed is subcritical, $w < w_{cr}$, the dark soliton is absolutely unstable, and when $w > w_{cr}$, the dark soliton is convectively unstable. The soliton family is parameterized by its amplitude ν ; thus $\nu \mapsto w_{cr}(\nu)$ forms a *separatrix* between absolute and convective instabilities. The separatrix $w_{cr}(\nu)$ can also be interpreted as the speed at which an initially localized perturbation spreads in time. Thus a convective instability occurs when the background flow speed, carrying the perturbation's center of mass, exceeds the speed at which the perturbation spreads out.

In general, the determination of $w_{cr}(\nu)$ via (3.8) requires numerical computation. Even so, (3.8) are much easier to use than the general criteria because the general criteria depend on $\Omega_0(k)$ over the complex- k plane, whereas (3.8) only depend on $\Omega_0(k)$ for real k .

3.3. The separatrix in the shallow amplitude regime. The shallow amplitude asymptotics of the dispersion relation (2.13) enable us to explicitly compute Ω_k and Ω_{kk} , determine the critical wavenumber k_{cr} , and find the separatrix $w_{cr}(\nu)$ between absolute and convective instabilities. Here it is convenient to use the wavenum-

ber scaling (see Appendix A)

$$k = \nu^2 p.$$

The asymptotic dispersion relation (3.4) becomes

$$\begin{aligned}\Omega(p; w) &\sim -\nu^2 wp + \nu^3 \frac{p}{3} (2\sqrt{3}p - 3)^{1/2} + \nu^5 \frac{p^2(\sqrt{3} - p)}{6(2\sqrt{3}p - 3)^{1/2}} \\ &\doteq -\nu^2 wp + \nu^3 \Lambda_0(p) + \nu^5 \Lambda_1(p), \quad 0 < \nu \ll 1.\end{aligned}$$

The simplified criteria (3.8) give

$$\begin{aligned}k_{\text{cr}} &= \nu^2 p_{\text{cr}} = \nu^2 (p_0 + \nu^2 p_1) + O(\nu^6), \\ \Omega_{kk}(k_{\text{cr}}) &\sim \frac{1}{\nu} \Lambda_0''(p_0) + \nu [\Lambda_0'''(p_0)p_1 + \Lambda_1''(p_0)], \\ \Omega_k(k_{\text{cr}}; w_{\text{cr}}) &\sim -w_{\text{cr}} + \nu \Lambda_0'(p_0) + \nu^3 [\Lambda_0''(p_0)p_1 + \Lambda_1'(p_0)].\end{aligned}$$

Equating like coefficients of ν and using (3.8), yields the next proposition.

PROPOSITION 3.4. *The first order asymptotic approximation of the critical velocity and wavenumber is*

$$(3.9a) \quad w_{\text{cr}} = \underbrace{\nu}_{\text{KP}} + \underbrace{\frac{2\nu^3}{9}}_{\text{NLS correction}} + O(\nu^5),$$

$$(3.9b) \quad k_{\text{cr}} = \underbrace{\frac{2\nu^2}{\sqrt{3}}}_{\text{KP}} + \underbrace{\frac{\nu^4}{3\sqrt{3}}}_{\text{NLS correction}} + O(\nu^6).$$

For comparison, Figure 3.4 shows the numerical solution of the system (3.8) and the asymptotics in (3.9). The numerical details are presented in section 5.1.

3.4. Convective/absolute instabilities of spatial dark solitons. The natural reference frame for studying the convective or absolute nature of soliton instabilities is the one moving with the soliton. In this reference frame, both the soliton density and velocity are independent of time. The dark soliton is referred to as a *spatial dark soliton*. Such structures arise, for example, in the context of flow past an impurity [9, 38], flow over extended obstacles, and dispersive shock waves [39, 22].

The spatial dark soliton in (2.1) satisfies $v = 0$, i.e.,

$$(3.10) \quad \cos \phi = \frac{c \sin \beta - d \cos \beta}{\sqrt{\rho}}.$$

This soliton is uniquely determined by four parameters rather than five. We use the background density ρ and background velocity (c, d) as three of these parameters along with the soliton angle $0 < \beta \leq \pi/2$. The normalized soliton amplitude $0 < \nu = |\sin \phi| = \sqrt{1 - \cos^2 \phi} \leq 1$ is then determined via (3.10) as

$$(3.11) \quad \sqrt{\rho} \sqrt{1 - \nu^2} = c \sin \beta - d \cos \beta.$$

The spatial dark soliton exhibits either an absolute or a convective instability depending on the Mach number of the background flow (2.2) and the amplitude ν . By

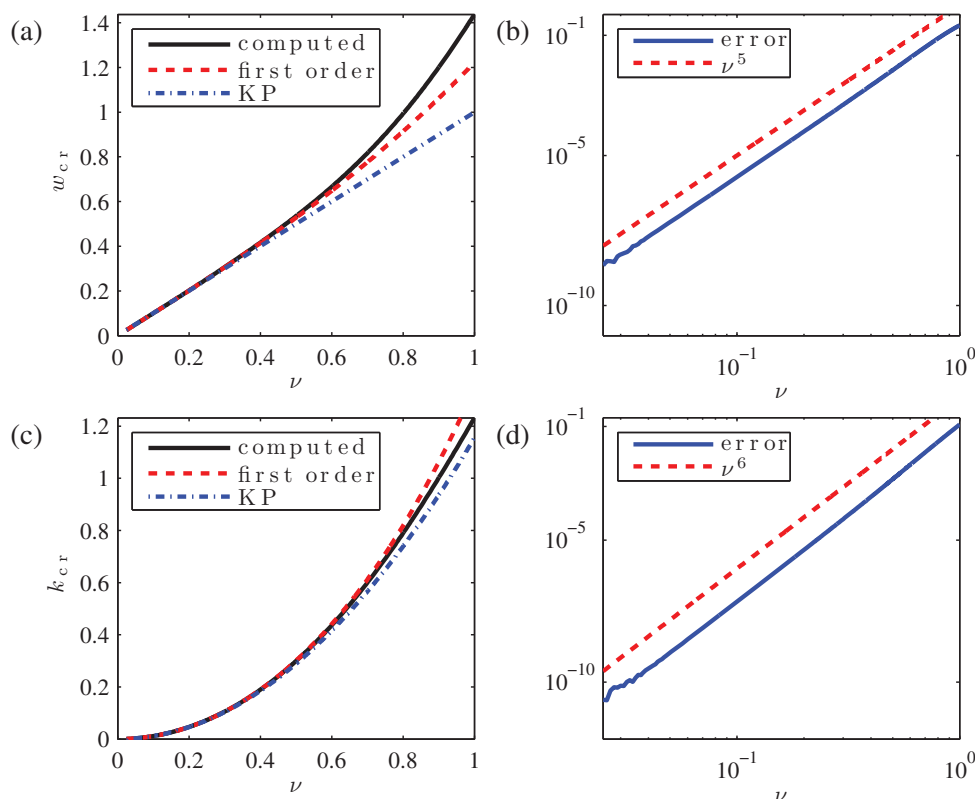


FIG. 3.4. (a) The separatrix $w_{\text{cr}}(\nu)$ between absolute and convective instabilities. For speeds $w \geq w_{\text{cr}}$ ($w < w_{\text{cr}}$), the dark soliton is convectively (absolutely) unstable. (c) The critical wavenumber k_{cr} satisfying the condition (3.7a). (b) and (d) are the differences in the numerically computed values of w_{cr} , k_{cr} and the first order approximations in (3.9a) and (3.9b), respectively, showing the expected error scalings.

moving in the reference frame $\xi = x - \kappa t$ of the normalized dark soliton (2.4), the background flow has velocity $-\kappa$ normal to the soliton and velocity $-w$ parallel to the soliton. The critical Mach number of the background flow and its first order asymptotic approximation are

$$(3.12a) \quad M_{\text{cr}}(\nu) = \sqrt{\kappa^2 + w_{\text{cr}}(\nu)^2} = \sqrt{1 - \nu^2 + w_{\text{cr}}(\nu)^2}$$

$$(3.12b) \quad \stackrel{(3.9a)}{=} 1 + \frac{2}{9}\nu^4 + O(\nu^6).$$

Transverse perturbations are absolutely unstable for $M < M_{\text{cr}}$ and convectively unstable for $M \geq M_{\text{cr}}$.

Figure 3.5 shows the numerically calculated dependence of M_{cr} on ν and comparisons with the asymptotic result (3.12b). Combining the asymptotic result (3.12b) with these computations leads to the following conclusion.

CONCLUSION 3.5. *The transition between convective and absolute instabilities for spatial dark solitons occurs at supersonic speeds for any soliton amplitude, i.e., $M_{\text{cr}}(\nu) > 1$. A sufficient condition for a spatial dark soliton with background Mach number M to be absolutely unstable is*

$$M \leq 1.$$

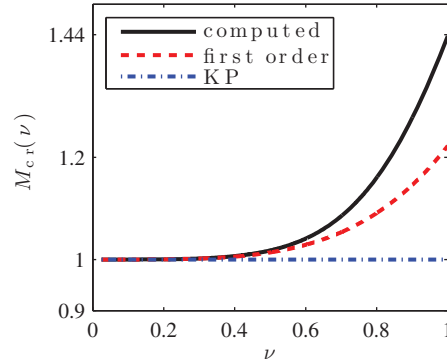


FIG. 3.5. Critical Mach number M_{cr} ((3.12a)) and its asymptotic approximations ($M_{\text{cr}} = 1$ for KP, (3.12b) for the first order correction) as functions of the soliton amplitude ν . For $M \geq M_{\text{cr}}$, the spatial dark soliton is convectively unstable; otherwise it is absolutely unstable.

A sufficient condition for a spatial dark soliton with background Mach number M to be convectively unstable is

$$M \geq M_{\text{cr}}(\nu = 1) \approx 1.4374.$$

Additionally, $\nu \mapsto M_{\text{cr}}(\nu)$ is monotonically increasing. In sum,

$$(3.13) \quad 1 < M_{\text{cr}} \lesssim 1.4374.$$

Remark 3.6. In [11], the bounds $1 \lesssim M_{\text{cr}} \lesssim 1.46$ were obtained. The leading order term in (2.13) was used to show that $M_{\text{cr}} \sim 1$ in the shallow regime. Equation (3.12b) improves the lower bound on M_{cr} and demonstrates that M_{cr} is strictly supersonic for all finite soliton amplitudes. The upper bound 1.46 in [11] was calculated from a rational approximation of the spectrum for large soliton amplitudes [29]. Equation (3.13) gives the accurate upper bound.

4. Oblique dispersive shock waves. In a dispersive fluid where dissipation is negligible, a jump in the density/velocity may be resolved by an expanding oscillatory region called a dispersive shock wave. The Whitham averaging technique [40] has been successfully used to describe a DSW's long time asymptotic behavior in a number of physical systems, for example, [41, 42, 17, 43, 44]. We briefly recap the rudiments of DSW theory. A DSW is a modulated wavetrain composed of a large-amplitude soliton edge and a small-amplitude, oscillatory edge, each moving with different speeds. In the relatively simple case where a DSW connects two constant states, the speeds associated with each edge are determined by jump conditions [45], in analogy with the Rankine–Hugoniot jump conditions of classical viscous gas dynamics. The jump conditions result from a simple wave solution of the Whitham modulation equations connecting the zero-wavenumber soliton edge to the zero-amplitude oscillatory edge. The existence of a DSW for a particular jump in the fluid variables is guaranteed when an appropriate entropy condition is satisfied. For a left-going DSW, we define the leading (trailing) edge to be the leftmost (rightmost) edge—and vice versa for a right-going DSW. The sign of the dispersion determines the locations of the soliton and small-amplitude edges. For systems with positive dispersion such as the NLS equation (1.1), the soliton is a depression wave that resides at the trailing edge of the DSW.

While DSWs in (1+1)-dimensions have been well studied, the theory of supersonic dispersive fluid dynamics in multiple spatial dimensions is in its infancy. Perhaps the

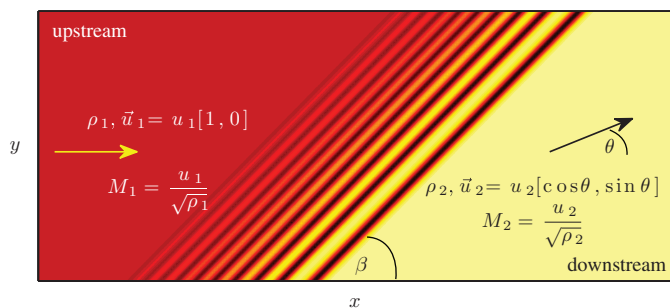


FIG. 4.1. Schematic of an oblique DSW.

simplest DSW in multiple dimensions is an oblique DSW, which has been studied in the stationary [46, 47, 48, 39] and nonstationary [22] regimes (see Figures 4.1 and 4.4). In this section, the analysis from the previous section is applied to the stationary and nonstationary oblique DSW soliton trailing edge to determine the separatrix between convective and absolute instabilities. In addition, in the weak shock and hypersonic regimes, we find that the jump conditions for stationary and nonstationary oblique DSWs are the same. As in classical gas dynamics, oblique DSWs can serve as building blocks for more complicated boundary value problems. Therefore, understanding the instability properties of oblique DSWs is important and relevant to supersonic dispersive flows. This has been further demonstrated by recent numerical simulations of NLS supersonic flow past a corner [39, 22].

In section 4.1, the jump conditions and instability properties of nonstationary oblique DSWs are presented. Section 4.2 contains a derivation of a stationary oblique DSW in the shallow regime, its stability, and comparisons with numerical simulation. Finally, section 4.3 demonstrates the connections between stationary and nonstationary oblique DSWs.

4.1. Nonstationary oblique DSWs. In this section, we first recap the derivation of a nonstationary oblique DSW [22] and then discuss its instability properties.

A schematic of a nonstationary oblique DSW at a specific time in its evolution is depicted in Figure 4.1. An incoming upstream, supersonic flow is turned through the oblique DSW by the deflection angle θ . To accommodate the deflection, the oblique DSW expands along the wave angle β . The leading edge consists of small-amplitude waves propagating into the upstream flow, while the trailing edge is composed of a dark soliton whose amplitude and speed are asymptotically calculated from the oblique DSW jump conditions.

The nonstationary oblique DSW results from the long time evolution of an initial jump in the density and velocity component normal to the DSW wave angle β , in the direction $\hat{n}_\beta = (\sin \beta, -\cos \beta)$, and continuity of the velocity parallel to β , in the direction $\hat{p}_\beta = (\cos \beta, \sin \beta)$. We consider the upstream state

$$\lim_{x \rightarrow -\infty} \rho = \rho_1, \quad \lim_{x \rightarrow -\infty} \vec{u} = (u_1, 0)$$

and the downstream state

$$\lim_{x \rightarrow +\infty} \rho = \rho_2, \quad \lim_{x \rightarrow +\infty} \vec{u} = (u_2 \cos \theta, u_2 \sin \theta).$$

The normal 1-DSW associated with the dispersionless characteristic $\lambda_1 = u - \sqrt{\rho}$

(left-going wave) satisfies the simple wave condition [42]

$$(4.1) \quad \hat{n}_\beta \cdot (u_1 - u_2 \cos \theta, -u_2 \sin \theta) = 2(\sqrt{\rho_2} - \sqrt{\rho_1}).$$

An NLS-governed fluid experiences potential flow (see (1.2)). By restricting the spatial variation of the solution to the direction \hat{n}_β and integrating the irrotationality constraint $v_x = u_y$ along the direction \hat{p}_β , we obtain the continuity of the parallel velocity component

$$(4.2) \quad \hat{p}_\beta \cdot (u_1 - u_2 \cos \theta, -u_2 \sin \theta) = 0.$$

Choosing the reference frame in which the soliton trailing edge is fixed, the speed of the soliton edge satisfies [42]

$$(4.3) \quad \hat{n}_\beta \cdot (u_1, 0) - \sqrt{\frac{\rho_2}{\rho_1}} = 0.$$

The jump conditions (4.1), (4.2), and (4.3) for the oblique DSW relate the upstream quantities ρ_1 , u_1 and one of the angles θ or β to the downstream quantities ρ_2 , u_2 and the other angle. Introducing the Mach numbers $M_j = u_j/\sqrt{\rho_j}$, $j = 1, 2$, along with some manipulation, the jump conditions become [22]

$$(4.4a) \quad \tan(\beta - \theta) = \frac{2}{M_1} \sec \beta - \tan \beta,$$

$$(4.4b) \quad M_2 = \frac{\cot \beta}{\cos(\beta - \theta)} = \frac{\sqrt{M_1^2 + 4 - 4M_1 \sin \beta}}{M_1 \sin \beta},$$

$$(4.4c) \quad \rho_2 = \rho_1 M_1^2 \sin^2 \beta.$$

Further manipulations lead to the equivalent relations

$$\frac{\sin(2\beta - \theta)}{\cos(\beta - \theta)} = \frac{2}{M_1}, \quad \cos \theta = \frac{M_1 \cos(2\beta) + 2 \sin \beta}{\sqrt{4 + M_1^2 - 4M_1 \sin \beta}}.$$

The associated entropy condition is $\rho_2 > \rho_1$, which, when incorporated into the jump conditions, gives

$$M_1 > 1, \quad 0 \leq \theta \leq \pi, \quad \sin^{-1} \frac{1}{M_1} \leq \beta \leq \frac{\pi}{2}.$$

These state that the upstream flow must be supersonic, the flow always turns *into* the DSW, and the wave angle is larger than the Mach angle $\sin^{-1}(1/M_1)$. The Mach angle is half the opening angle of the Mach cone, inside which infinitesimally small disturbances are confined to propagate in dispersionless supersonic flow. A convenient way to visualize these results is by the M - θ - β diagram in Figure 4.2 that relates the deflection and wave angles for a given upstream Mach number M_1 . Figure 4.2 includes the sonic curve $M_2 = 1$ (to the right/left the flow is sub/supersonic).

A natural question is whether oblique DSWs with supersonic downstream flow conditions are convectively or absolutely unstable. To address this question, we use the next definition.

DEFINITION 4.1. *Transverse perturbations to the nonstationary and stationary oblique DSW are convectively (absolutely) unstable whenever the trailing dark soliton edge is convectively (absolutely) unstable.*

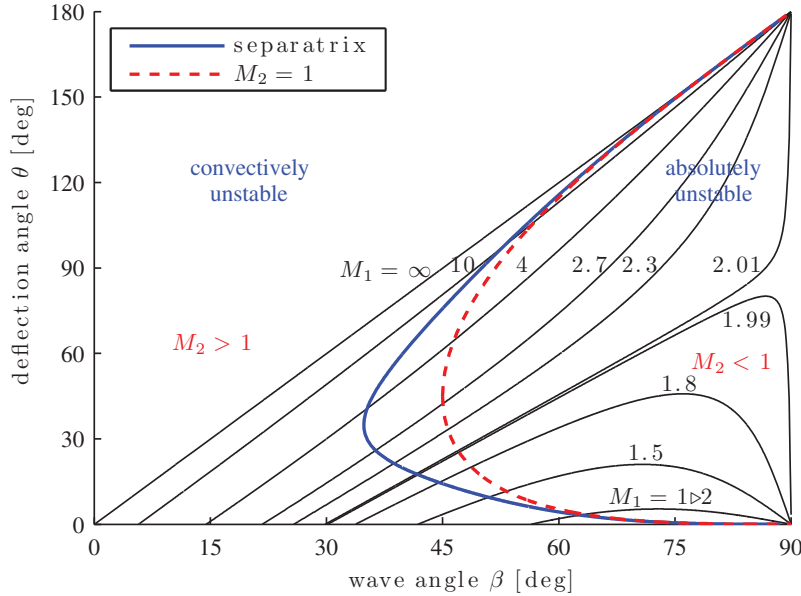


FIG. 4.2. The M - θ - β diagram for nonstationary oblique DSWs of the NLS equation (1.1). Each upstream Mach number M_1 leads to a relationship between θ and β . The separatrix curve (solid) between convectively and absolutely unstable solitons is supersonic, i.e., in the $M_2 > 1$ region (left of the sonic line, dashes). The separatrix curve is asymptotic to the sonic line as $\beta \rightarrow 90^\circ$.

See further discussion in section 6.

Spatial dark solitons exhibit the constraint (3.10). When applied to the oblique DSW trailing edge in Figure 4.1 with background flow parameters $(c, d) = \sqrt{\rho}M_2(\cos \theta, \sin \theta)$, we find

$$\cos \phi = M_2 \sin(\beta - \theta).$$

Using the jump conditions in (4.4), we determine the normalized soliton amplitude

$$(4.5) \quad \nu(M_1, \theta) = \sin \phi = \frac{2\sqrt{M_1 \sin \beta - 1}}{M_1 \sin \beta},$$

where β is related to θ by (4.4a). The Mach number of the downstream flow adjacent to the soliton is M_2 so the absolute/convective stability criterion (3.12a) determines the separatrix

$$(4.6) \quad M_2(M_1, \theta) = M_{\text{cr}}(\nu) = \sqrt{1 - \nu^2 + w_{\text{cr}}(\nu)^2}$$

with ν given in (4.5). Conclusion 3.5 implies the next corollary.

COROLLARY 4.2. *Nonstationary oblique DSWs with subsonic downstream flow are absolutely unstable. Supersonic downstream flow can be either convectively or absolutely unstable.*

This conclusion can also be gleaned from Figure 4.2. To the right of the separatrix, the trailing edge oblique soliton is absolutely unstable because $M_2 < M_{\text{cr}}$, while to its left, the soliton is convectively unstable. The region to the right of the separatrix and to the left of the sonic line represents absolutely unstable oblique DSWs with supersonic downstream flow conditions. Below we derive additional properties of the separatrix.

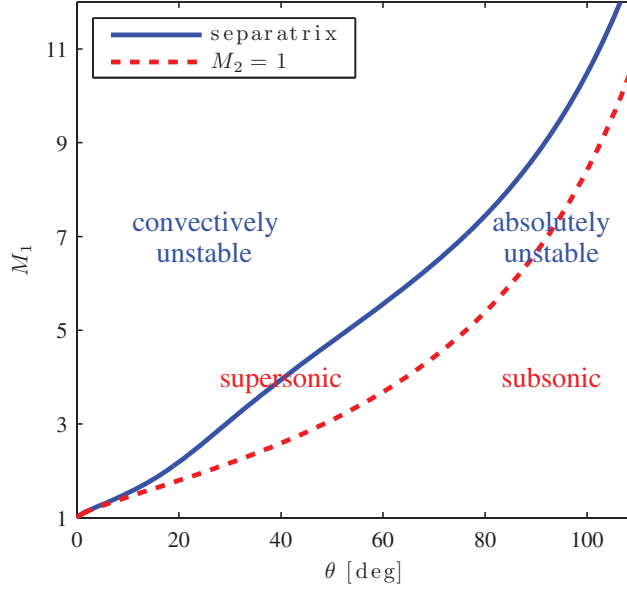


FIG. 4.3. Separatrix curve (solid) dividing the M_1 - θ plane for nonstationary oblique DSWs into two regions: the absolute/convective instability of the trailing edge dark soliton. The sonic curve $M_2(M_1, \theta) = 1$ (dashed) is included for comparison.

From Figure 4.2, we observe a minimum wave angle β_{cr} , below which the oblique DSW is convectively unstable. Setting $M_2 = M_{\text{cr}}$ in (4.4b) and solving for β we find

$$\sin \beta_{\text{cr}} = \frac{-2 + \sqrt{4 + (4 + M_1^2)M_{\text{cr}}^2}}{M_1 M_{\text{cr}}^2},$$

which has a minimum for $M_1 = 2\sqrt{1 + M_{\text{cr}}^2}$, $M_{\text{cr}} = M_{\text{cr}}(\nu = 1) \approx 1.4374$. We therefore have a sufficient condition for the oblique DSW trailing edge to be convectively unstable

$$\beta \leq \beta_{\text{cr}} = \sin^{-1} \left[(1 + M_{\text{cr}}(1)^2)^{-1/2} \right] \approx 34.83^\circ.$$

The nonstationary oblique DSW is uniquely determined by the parameters M_1 , θ , and ρ_1 . Thus, given $M_1 > 1$ and $0 < \theta < \pi$, the absolute or convective instability of the corresponding oblique DSW's trailing edge is determined by the location of (M_1, θ) relative to the separatrix condition (4.6) in the M_1 - θ plane, as shown in Figure 4.3. The parameter ρ_1 does not affect the absolute or convective nature of the instability.

Using the small-amplitude result (3.12a), $M_{\text{cr}} \sim 1 + \frac{2}{9}\nu^4$, assuming near sonic upstream flow $M_1 = 1 + \varepsilon$, $0 < \varepsilon = \mathcal{O}(\nu^2) \ll 1$, and expanding β , θ , M_2 , and M_{cr} , we compute the critical angle

$$\begin{aligned} M_2(1 + \varepsilon, \theta_{\text{cr}}) &= M_{\text{cr}} + \mathcal{O}(\varepsilon^3) = M_{\text{cr}} + \mathcal{O}(\nu^6), \\ \theta_{\text{cr}} &\sim \frac{4}{3\sqrt{3}}\varepsilon^{3/2} \left(1 - \frac{26}{27}\varepsilon \right), \quad 0 < \varepsilon \ll 1. \end{aligned}$$

For $\theta \leq \theta_{\text{cr}}$, the trailing edge dark soliton is convectively unstable and absolutely

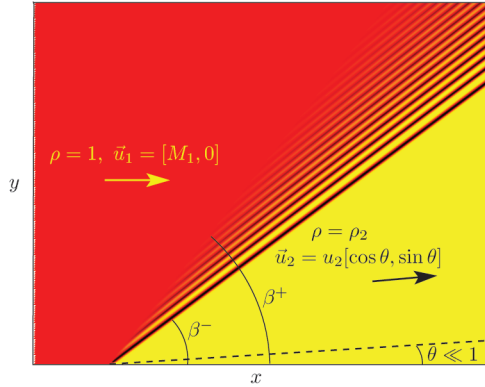


FIG. 4.4. Example spatial oblique DSW with small deflection angle θ constructed from the asymptotic solution (4.14).

unstable otherwise. Similarly, the sonic angle satisfies

$$M_2(1 + \varepsilon, \theta_{\text{sonic}}) = 1 + \mathcal{O}(\varepsilon^3) = 1 + \mathcal{O}(\nu^6),$$

$$\theta_{\text{sonic}} \sim \frac{4}{3\sqrt{3}} \varepsilon^{3/2} \left(1 - \frac{2}{3} \varepsilon\right), \quad 0 < \varepsilon \ll 1.$$

For $\theta < \theta_{\text{sonic}}$, the downstream flow is supersonic and subsonic when $\theta > \theta_{\text{sonic}}$. For the narrow window of deflection angles $\theta_{\text{cr}} < \theta < \theta_{\text{sonic}}$, the flow is supersonic and absolutely unstable.

4.2. Spatial oblique DSWs. We have so far focused on nonstationary oblique DSWs. In this section, we construct *stationary* or spatial oblique DSWs in the weakly nonlinear regime (see Figure 4.4), study their instability properties, and perform numerical simulations. This discussion for the NLS equation (1.1) with positive dispersion parallels the developments in [46, 47] applied to ion-acoustic waves in plasma, a system with negative dispersion.

Equations (1.3a) and (1.3b), and the irrotationality constraint due to potential flow are considered in the (2+0)-dimensional case

$$(4.7a) \quad (\rho u)_x + (\rho v)_y = 0,$$

$$(4.7b) \quad uu_x + vv_y + \rho_x = \frac{1}{4} \left(\frac{\rho_{xx} + \rho_{yy}}{\rho} - \frac{\rho_x^2 + \rho_y^2}{2\rho^2} \right)_x,$$

$$(4.7c) \quad v_x - u_y = 0.$$

We seek a special class of solutions that are related to supersonic flow past a sharp corner or wedge. For this, we treat y as a time-like variable and consider the “initial conditions” at $y = 0$

$$(4.8a) \quad \rho(x, 0) = \begin{cases} 1, & x < 0, \\ \rho_2, & x > 0, \end{cases}$$

$$(4.8b) \quad u(x, 0) = \begin{cases} M_1, & x < 0, \\ \sqrt{\rho_2} M_2 \cos \theta, & x > 0, \end{cases}$$

$$(4.8c) \quad v(x, 0) = \begin{cases} 0, & x < 0, \\ \sqrt{\rho_2} M_2 \sin \theta, & x > 0. \end{cases}$$

The well-posedness of this initial value problem is plausible in the supersonic regime, $M_j > 1$, $j = 1, 2$, due to the hyperbolicity of the dispersionless equations (see, e.g., [27]). We seek a stationary, oblique DSW solution in the supersonic and weakly nonlinear regime $0 < \rho_2 - 1 \ll 1$. For this, we apply the method of multiple scales

$$(4.9a) \quad \rho = 1 + \varepsilon \rho^{(1)} + \varepsilon^2 \rho^{(2)} + \dots,$$

$$(4.9b) \quad u = M_1 - \varepsilon u^{(1)} + \varepsilon^2 u^{(2)} + \dots,$$

$$(4.9c) \quad v = \varepsilon v^{(1)} + \varepsilon^2 v^{(2)} + \dots$$

in the transformed variables

$$(4.10) \quad \xi = \varepsilon^{1/2}[x - (M_1^2 - 1)^{1/2}y], \quad \tau = \varepsilon^{3/2}y.$$

This particular choice is motivated by the line $\xi = \text{const}$ whose angle with the x axis is the Mach angle $\sin^{-1}(1/M_1)$ for small-amplitude wave propagation in the upstream flow. Equating like powers of ε leads to

$$\begin{aligned} -u_\xi^{(1)} + M_1 \rho_\xi^{(1)} - (M_1^2 - 1)^{\frac{1}{2}} v_\xi^{(1)} &= 0, \\ \mathcal{O}(\varepsilon^{\frac{3}{2}}): \quad -M_1 u_\xi^{(1)} + \rho_\xi^{(1)} &= 0, \\ v_\xi^{(1)} - (M_1^2 - 1)^{\frac{1}{2}} u_\xi^{(1)} &= 0. \end{aligned}$$

The solution incorporating the initial conditions (4.8) is

$$(4.11) \quad \rho^{(1)} = M_1 u^{(1)}, \quad v^{(1)} = (M_1^2 - 1)^{\frac{1}{2}} u^{(1)}$$

with $u^{(1)}$ determined at the next order:

$$\begin{aligned} u_\xi^{(2)} + M_1 \rho_\xi^{(2)} - (M_1^2 - 1)^{\frac{1}{2}} v_\xi^{(2)} - (\rho^{(1)} u^{(1)})_\xi \\ + v_\tau^{(1)} - (M_1^2 - 1)^{\frac{1}{2}} (\rho^{(1)} v^{(1)})_\xi &= 0, \\ \mathcal{O}(\varepsilon^{\frac{5}{2}}): \quad M_1 u_\xi^{(2)} + \rho_\xi^{(2)} + u^{(1)} u_\xi^{(1)} + (M_1^2 - 1)^{\frac{1}{2}} v^{(1)} u_\xi^{(1)} &= \frac{1}{4} \rho_{\xi\xi\xi}^{(1)}, \\ v_\xi^{(2)} + (M_1^2 - 1)^{\frac{1}{2}} u_\xi^{(2)} + u_\tau^{(1)} &= 0. \end{aligned}$$

Inserting (4.11) we obtain the KdV equation

$$(4.12) \quad u_\tau^{(1)} - \frac{3M_1^3}{2(M_1^2 - 1)^{\frac{1}{2}}} u^{(1)} u_\xi^{(1)} + \frac{M_1^2}{8(M_1^2 - 1)^{\frac{1}{2}}} u_{\xi\xi\xi}^{(1)} = 0.$$

It is convenient to consider the transformed variables U, ζ as

$$(4.13) \quad U = -\frac{3M_1^{\frac{7}{3}}}{(M_1^2 - 1)^{\frac{1}{3}}} u^{(1)} + 1, \quad \xi = \frac{M_1^{\frac{2}{3}}(\zeta - \tau)}{2(M_1^2 - 1)^{\frac{1}{6}}}.$$

Then, (4.12) becomes the KdV equation with negative dispersion

$$U_\tau + UU_\zeta + U_{\zeta\zeta\zeta} = 0.$$

The initial data in (4.8) maps to the Riemann problem

$$U(\zeta, 0) = \begin{cases} 1, & \zeta < 0, \\ 0, & \zeta > 0. \end{cases}$$

This *dispersive* Riemann problem was solved by Gurevich and Pitaevskii in 1974 [41]. The result is a DSW with the trailing edge, small-amplitude wave speed $c_T = -1$ and leading edge, soliton speed $c_L = 2/3$. The leading edge soliton amplitude is 2, corresponding to the KdV soliton speed/amplitude relation. The oscillatory part of

the DSW, for τ sufficiently large, has the approximate form [41, 15]

$$(4.14) \quad U(\zeta, \tau) \sim m(\zeta/\tau) - 1 + 2\operatorname{dn}^2 \left(\frac{K[m(\zeta/\tau)]}{\pi} \phi(\zeta, \tau); m(\zeta/\tau) \right), \quad \tau \gg 1,$$

where dn is a Jacobi elliptic function and $K[m]$ is the complete elliptic integral of the first kind. The elliptic parameter $m(\zeta/\tau)$ is the self-similar, simple wave solution to the Whitham modulation equations given implicitly by

$$\frac{\zeta}{\tau} = \frac{1}{3}(1+m) - \frac{2}{3}m \frac{(1-m)K[m]}{E[m] - (1-m)K[m]},$$

where $E[m]$ is the complete elliptic integral of the second kind. The phase is determined through

$$\phi(\zeta, \tau) = -\frac{\pi\tau}{\sqrt{6}} \int_{\zeta/\tau}^{2/3} \frac{dz}{K[m(z)]}.$$

To obtain the NLS oblique DSW solution in its unscaled form, we use the transformations (4.13), (4.10) along with the substitutions (4.11) to match the asymptotic solution (4.9) to the initial conditions (4.8). The deflection angle θ is related to the small parameter ε via

$$(4.15) \quad \theta \sim \varepsilon \frac{(M_1^2 - 1)^{\frac{5}{6}}}{3M_1^{\frac{10}{3}}} \ll 1,$$

so that weak spatial DSWs correspond to a small DSW deflection angle. Then the relationship between the downstream and upstream variables takes the asymptotic form

$$(4.16a) \quad \rho_2 \sim 1 + \frac{M_1^2}{(M_1^2 - 1)^{\frac{1}{2}}} \theta,$$

$$(4.16b) \quad M_2 \sim M_1 \left(1 - \frac{M_1^2 + 2}{2(M_1^2 - 1)^{\frac{1}{2}}} \theta \right), \quad 0 < \theta \ll 1.$$

The KdV DSW speeds $c_T = -1$ and $c_L = 2/3$ correspond to the slopes of the oscillatory region's boundaries which we transform to the leading and trailing angles β_+ , β_- , respectively, for the stationary oblique DSW. Using the transformations (4.10), (4.13), and (4.15), the oblique DSW angles take the asymptotic forms

$$(4.17a) \quad \beta_- \sim \sin^{-1} \left(\frac{1}{M_1} \right) + \frac{M_1^2}{2(M_1^2 - 1)} \theta,$$

$$(4.17b) \quad \beta_+ \sim \sin^{-1} \left(\frac{1}{M_1} \right) + \frac{3M_1^2}{M_1^2 - 1} \theta, \quad 0 < \theta \ll 1.$$

Finally, the trailing edge soliton amplitude and phase jump 2ϕ with the angle β_- have the asymptotic form

$$(4.18) \quad \rho_2 - \rho(x, x \tan \beta_-) = \sqrt{\rho_2} \sin \phi \sim \phi \sim \frac{2M_1^2}{(M_1^2 - 1)^{\frac{1}{2}}} \theta.$$

This DSW solution is plotted in Figure 4.4 and approximates a stationary, weak oblique DSW for NLS.

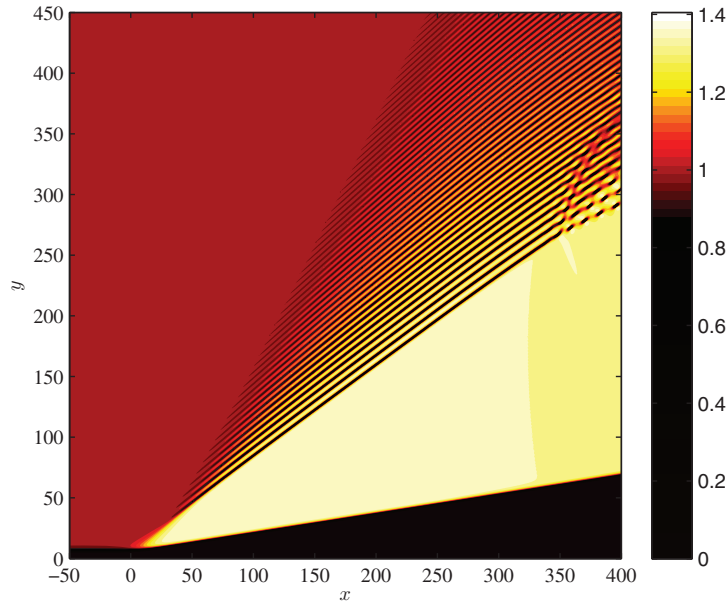


FIG. 4.5. Numerical simulation of supersonic flow past a corner with $\theta = 9^\circ$, $M_1 = 2$, at $t = 400$. The color scale is chosen to visually resolve the small amplitude oscillations.

Equations (4.16) and (4.17) are the jump conditions for weak, stationary oblique DSWs. These can be used to approximately solve the problem of supersonic flow over a corner with angle $0 < \theta \ll 1$. Additionally, due to symmetry arguments, two stationary oblique DSWs approximately solve supersonic flow over a wedge as in [39]. Figure 4.5 shows the numerical solution of (1.1) for supersonic $M_1 = 2$ flow past a corner with angle $\theta = 9^\circ$ after the flow pattern has reached a quasi-steady state. (See section 5.2 for the numerical details.) Sufficiently close to the corner, the structure of the numerical solution resembles the asymptotic oblique DSW shown in Figure 4.4. Further away from the corner, the first sign of instability occurs along the trailing dark soliton edge leading to the generation of vortices. This provides some justification for our definition of oblique DSW instability in Definition 4.1. Furthermore, we observe that the vortices are convected further away from the corner as time progresses.¹ In a previous work [22], we performed numerical simulations of NLS supersonic flow past a corner for a large number of flow configurations, observing similar, stable pattern formation in some cases. Flow configurations where the instability overwhelms any stable pattern formation were also observed. We identify these two flow regimes with convective and absolute instability of the oblique DSW.

Table 4.1 summarizes the asymptotic estimates in (4.16) and (4.17) compared with the numerical computations showing excellent agreement, even for fairly large corner angles and when the “small” parameter ε is larger than one.

¹The vortex pattern eventually stabilizes at a fixed distance from the corner. A recent study [49] of NLS dark soliton convective/absolute instabilities has some independent results that overlap with ours in sections 3.2 and 3.4. This work also gives a further description of perturbation convection along the soliton. The effective group velocity of the perturbation along the soliton is found to be equal to the critical flow speed (here $\sqrt{\rho_2} w_{cr}$). However, convective instability theory does not explain the numerically observed stabilization of vortex formation at a fixed distance from the corner.

TABLE 4.1

Comparison of the asymptotic results of (4.16) and (4.17) and numerical simulation of supersonic flow over a corner.

$M_1 = 2$	θ	ε	M_2	ρ_2	β^-	β^+
Theory	3°	0.6	1.82	1.12	32°	42°
Numerics	3°	0.6	1.84	1.12	32°	39°
Theory	6°	1.3	1.64	1.24	34°	54°
Numerics	6°	1.3	1.67	1.26	34°	49°
Theory	9°	1.9	1.46	1.36	36°	66°
Numerics	9°	1.9	1.51	1.40	37°	62°

The trailing edge dark soliton is shallow. Therefore, using the theory developed in section 3.3 and (4.16b), (3.12b), the oblique DSW is convectively unstable when

$$M_2 > M_{\text{cr}}(\nu) \quad \text{or} \quad M_1[1 + \mathcal{O}(\theta)] > 1 + \mathcal{O}(\theta^4), \quad 0 < \theta \ll 1,$$

because $\nu = \sin \phi \sim \mathcal{O}(\theta)$ from (4.18). As long as $M_1 > 1$, independent of the corner angle θ , using Conclusion 3.5 gives the next corollary.

COROLLARY 4.3. *For NLS supersonic upstream flow $M_1 > 1$ and sufficiently small corner angles $0 < \theta \ll 1$, the oblique DSW emanating from a sharp corner is convectively unstable.*

4.3. Relationship between stationary and nonstationary oblique DSWs.

As shown in the previous section, stationary oblique DSWs can be physically realized as the solution of a two-dimensional *boundary value problem* involving supersonic flow. In contrast, the nonstationary oblique DSW studied in section 4.1 results from the solution of an *initial value problem*. As we now demonstrate, the downstream flow conditions for the stationary and nonstationary oblique DSW are the same in two asymptotic regimes: weak shocks and hypersonic flow.

The downstream flow conditions and the stationary trailing edge soliton in both the stationary and nonstationary oblique DSWs are characterized by the deflection angle θ , the wave angle β^- or β for the nonstationary case, the Mach number M_2 , and the density ρ_2 . These properties are related via the oblique DSW jump conditions. For weak oblique DSWs, we assume a fixed upstream supersonic Mach number $M_1 > 1$ and small deflection angle $0 < \theta \ll 1$ as in section 4.2. By a standard asymptotic calculation, an expansion of the jump conditions for the nonstationary oblique DSW in (4.4) in the form

$$\rho_1 = 1, \quad \rho_2 = 1 + \mathcal{O}(\theta), \quad M_2 = M_1 + \mathcal{O}(\theta), \quad \beta = \sin^{-1} 1/M_1 + \mathcal{O}(\theta),$$

gives precisely the same result as that obtained for the stationary oblique DSW in (4.16a), (4.16b), and (4.17a).

The hypersonic regime assumes the large Mach number scaling $M_1 \gg 1$ and small deflection angle $\theta = \mathcal{O}(1/M_1)$. In this asymptotic regime, the jump conditions (4.4) become

$$(4.19a) \quad \rho_2 = \left(\frac{\theta M_1}{2} + 1 \right)^2 + \mathcal{O}(1/M_1),$$

$$(4.19b) \quad M_2 = \frac{2M_1}{2 + \theta M_1} + \mathcal{O}(1),$$

$$(4.19c) \quad \beta = \frac{\theta}{2} + \frac{1}{M_1} + \mathcal{O}(1/M_1^2), \quad M_1 \gg 1, \quad 0 < \theta = \mathcal{O}(1/M_1),$$

where we have assumed that $\rho_1 = 1$. In [48, 39], stationary oblique DSW solutions of (4.7) and (4.8) in the hypersonic regime were constructed asymptotically. The classical notion of hypersonic similitude [50] applies so that the (2+0)-dimensional stationary problem was asymptotically mapped to a (1+1)-dimensional problem for the NLS equation. Stationary, supersonic flow past an extended obstacle is then related to a piston problem, which can be solved analytically in the case of a sharp corner (constant piston speed) [51] and for more general profiles [39, 52]. The results for the stationary oblique DSW are the same as those computed asymptotically for the nonstationary case in (4.19) when $M_1\theta \leq 2$. The case $M_1\theta > 2$ corresponds to a novel feature of the dispersive piston problem where the oblique DSW experiences cavitation and the DSW forms an oscillatory wake [51], not captured by the jump conditions (4.4). Combining these results with Corollaries 4.2 and 4.3 demonstrates the next conclusion.

CONCLUSION 4.4. *For weak (small deflection angle $0 < \theta \ll 1$, fixed upstream Mach number M_1) or hypersonic ($M_1 \gg 1$, $\theta = \mathcal{O}(1/M_1)$, $M_1\theta \leq 2$) oblique DSWs, the nonstationary and stationary flows have the same asymptotic downstream flow properties and trailing edge soliton amplitudes/angles. In these regimes, the oblique DSWs are convectively unstable.*

5. Computational techniques. In this section, we present details of our numerical methods for computing the spectrum of transversely unstable perturbations as well as derivatives of the dispersion relation via adjoint methods (section 5.1). Direct numerical simulations of NLS supersonic flow over a corner are explained in section 5.2.

5.1. Computing the spectrum and derivatives of the dispersion relation. Accurately computing the spectrum of the linearized NLS equation (1.1), finding the maximal growth wavenumber (2.14) and the critical wavenumber (3.7a) require a fine grid and sufficiently large computational domain. This turns out to be challenging, especially in the small amplitude regime. To achieve this, we employ a combination of computational and analytical techniques explained below.

- The linearized operator in (2.7) is realized using the centered, fourth order (sparse) finite difference stencil in ξ for the Laplacian and other derivative operators. Zero Dirichlet boundary conditions are embedded into the associated matrix. We find that a domain size of $11/\nu$ serves well (increasing the domain size has negligible effect on the results).
- For accuracy, the number of grid points along the transverse direction ξ should scale as $1/\nu$. As ν decreases from 1 to 0.01, we use $2^9 - 2^{13}$ grid points. Using fewer points can lead to completely wrong results, either because $k_{\max} \rightarrow 0$ or because $k_{\text{cr}} \rightarrow k_{\text{cutoff}} +$ as $\nu \rightarrow 0$.
- The discrete eigenvalue $\Omega_0(k)$ and its associated localized eigenfunction $\mathbf{f}_0(\xi; k)$ are computed using MATLAB's sparse eigenvalue solver ('eigs' with 'SM').
- One approach is to compute $\Omega_0(k)$ on a grid of k values (as for Figure 2.1). Then, $\Omega'_0(k)$ (resp., $\Omega''_0(k)$) can be computed using finite differences and minimized on the k grid to find k_{\max} (resp., k_{cr}). This method turns out to be computationally expensive. To overcome these challenges, an accurate and fast method is explained below.

Recall the eigenvalue problem (2.7). As discussed previously the discrete spectrum of JL consists of two simple eigenvalues of opposite signs, $\pm\Omega_0(k)$ (we choose the positive sign), with the associated eigenfunction $\mathbf{f}_0(\xi; k)$. Our main goal is to compute k_{\max} such that $\Omega'_0(k_{\max}) = 0$ and k_{cr} such that $\Omega''_0(k_{\text{cr}}) = 0$. This is achieved using the following algorithm:

1. Compute the discrete spectrum at some (initial) k , i.e., $\Omega_0(k)$ and $\mathbf{f}_0(\xi; k)$.
2. Apply adjoint methods to find exact expressions for $\Omega'_0(k)$ and $\Omega''_0(k)$, i.e., (5.5)–(5.6) below.
3. Repeat steps 1–2 using a root finder to converge to k_{\max} and k_{cr} .
4. Compute $\Gamma_{\max} = \Im\{\Omega_0(k_{\max})\}$ and/or $\Omega_{\text{cr}} = \Omega_0(k_{\text{cr}})$ and $w_{\text{cr}} = \Omega'_0(k_{\text{cr}})$.

We proceed to derive the relevant expressions. Use will be made of the standard Pauli matrices,

$$(5.1) \quad \sigma_1 \doteq \begin{bmatrix} 0 & 1 \\ 1 & 0 \end{bmatrix}, \quad \sigma_2 \doteq \begin{bmatrix} 0 & -i \\ i & 0 \end{bmatrix}, \quad \sigma_3 \doteq \begin{bmatrix} 1 & 0 \\ 0 & -1 \end{bmatrix},$$

the reflection operator R , $Rg(x) = g(-x)$, and the adjoint of an operator will be denoted by $(\cdot)^\dagger$.

Differentiating (2.7) with respect to k gives

$$(5.2) \quad \left(\sigma_2 L_0 + \frac{1}{2} k^2 \sigma_2 + \Omega_0 \right) \mathbf{f}'_0 = -(k\sigma_2 + \Omega'_0) \mathbf{f}_0,$$

where $(\cdot)'$ denotes differentiation with respect to k . Solvability requires that $(k\sigma_2 + \Omega'_0) \mathbf{f}_0$ be orthogonal to the nullspace of the adjoint operator to the left-hand side of (5.2). In Appendix C we prove that this nullspace can be characterized as follows.

LEMMA 5.1. *For $k \in \mathbb{C} \setminus \{0, \pm k_{\text{cutoff}}\}$ and $(\Omega_0(k), \mathbf{f}_0(\xi; k))$ an eigenpair satisfying*

$$(5.3) \quad \left(\sigma_2 L_0 + \frac{1}{2} k^2 \sigma_2 + \Omega_0 \right) \mathbf{f}_0 = 0,$$

we have

$$(5.4) \quad \ker \left\{ \left(\sigma_2 L_0 + \frac{1}{2} k^2 \sigma_2 + \Omega_0 \right)^\dagger \right\} = \text{span}\{R\sigma_1 \mathbf{f}_0^*\}.$$

Using Lemma 5.1 and taking the inner product of (5.2) with $R\sigma_1 \mathbf{f}_0^*$, the solvability condition reads

$$(5.5) \quad \Omega'_0(k) = -k \frac{\langle \sigma_2 \mathbf{f}_0, R\sigma_1 \mathbf{f}_0^* \rangle}{\langle \mathbf{f}_0, R\sigma_1 \mathbf{f}_0^* \rangle}.$$

Differentiating (5.2) with respect to k gives

$$\left(\sigma_2 L_0 + \frac{1}{2} k^2 \sigma_2 + \Omega_0 \right) \mathbf{f}''_0 = -(k\sigma_2 + \Omega'_0) \mathbf{f}'_0 - (\sigma_2 + \Omega''_0) \mathbf{f}_0.$$

Using the solvability condition we conclude that

$$(5.6) \quad \Omega''_0(k) = -2 \frac{\langle (k\sigma_2 + \Omega'_0) \mathbf{f}'_0, R\sigma_1 \mathbf{f}_0^* \rangle}{\langle \mathbf{f}_0, R\sigma_1 \mathbf{f}_0^* \rangle} - \frac{\langle \sigma_2 \mathbf{f}_0, R\sigma_1 \mathbf{f}_0^* \rangle}{\langle \mathbf{f}_0, R\sigma_1 \mathbf{f}_0^* \rangle}.$$

In summary, we compute $\Omega'_0(k)$ and $\Omega''_0(k)$ using (5.2), (5.3), (5.5), and (5.6). These computations are accurate and fast. The most time-consuming operation is the computation of the discrete spectrum of L .

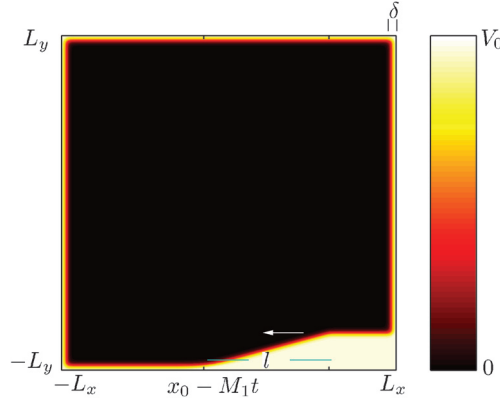


FIG. 5.1. An example potential $V(x, y, t)$ with $V_0 \gg 1$ used to model numerical simulation of supersonic flow past a corner. Regions where $V(x, y, t)$ is large correspond to negligible density. The ramp moves to the left with speed M_1 leading to oblique DSW formation.

5.2. Numerical solution of the NLS equation. In section 4.2 we presented the numerical solution of supersonic NLS flow past a corner. The technique used was the same as that presented in [22]. We introduce a linear potential with large contrast that acts as a penalization to flow outside the domain. Such volume penalization methods are well known in classical fluid dynamics (see, e.g., [53]). In the context of BEC and optics, superfluid flow around obstacles or boundaries is realized in practice using electromagnetic waves or a variable refractive index, both modeled as a spatially varying, linear potential. The benefits of this numerical technique include the use of a regular, Cartesian mesh and highly accurate pseudospectral derivative calculations.

The time-dependent NLS/GP equation (1.1) with a linear potential

$$(5.7) \quad i\psi_t = -\frac{1}{2}(\psi_{xx} + \psi_{yy}) + V(x, y, t)\psi + |\psi|^2\psi$$

was solved numerically using a pseudospectral, Fourier spatial discretization, and a fourth order Runge–Kutta explicit time stepper. These computations were performed on a rectangular mesh of $N_x N_y$ equispaced grid points within the domain $[-L_x, L_x] \times [-L_y, L_y]$. Our choice of the potential

$$(5.8a) \quad V(x, y, t) = V_0 \left[1 - H_\mu(L_x - |x| - \delta) H_\mu(L_y - |y| - \delta) \right]$$

$$(5.8b) \quad H_\mu(y - C(x - M_1 t)) \Big],$$

$$(5.8c) \quad C(\xi) = -\tan(\theta) \left[H_\mu(x_1 - \xi) - H_\mu(l) \right] - L_y + \delta,$$

$$(5.8d) \quad H_\mu(\xi) = \frac{1}{2} + \frac{1}{2} \tanh(\xi/\mu),$$

models the boundary conditions corresponding to flow over a corner and also serves to “localize” the solution so that a pseudospectral, Fourier discretization with periodic boundary conditions can be employed. An example potential is shown in Figure 5.1. The time-dependent potential corresponds to a moving ramp. The function H_μ is a regularized Heaviside step function with transition width μ . The terms on line (5.8a)

effect the localization of ψ to within δ of the domain boundaries. The terms on lines (5.8b) and (5.8c) correspond to a moving ramp with corner angle θ and apex located at $(x_0 - M_1 t, -L_y + \delta)$. When the second corner at $x = x_0 - M_1 t + l$ is reached, the ramp flattens and continues as a straight line. The initial condition is the nonlinear, stationary ground state of (5.7) with potential $V(x, y, 0)$ computed by the spectral renormalization technique [54] with the unit density constraint $|\psi(0, 0, 0)|^2 = 1$. The potential contrast V_0 is taken sufficiently large so that the density is effectively zero where $V(x, y, t) \approx V_0$. Time integration was carried out until the corner reached the left boundary. Near the corner, the flow approximates a “pure” oblique DSW as shown in Figure 4.5. Parameter values for Table 4.1 are $N_x = 4000$, $N_y = 1000$, $L_x = 2000$, $L_y = 500$, $V_0 = 20$, $\delta = 2$, $x_0 = 1000$, $l = 1000$, $\mu = 2$, and a time step of 0.05. The simulation depicted in Figure 4.5 results from $N_x = 3200$, $N_y = 1600$, $L_x = 800$, $L_y = 400$, $V_0 = 20$, $\delta = 2$, $x_0 = 400$, $l = 400$, $\mu = 2$, and a time step of 0.01.

6. Discussion and conclusions. One of the motivating questions for this study was the nature of convective versus absolute instabilities of dark solitons. In general, the characterization of the instability type requires knowledge of the dispersion relation for a range of wavenumbers in the complex plane. Unfortunately, the exact discrete spectrum (and hence dispersion relation) for NLS dark solitons is unknown. The formal analysis presented in [11] led to greatly simplified criteria for determining the instability type, which involve only the imaginary (stable) portion of the spectrum.

In this study, the underlying assumptions behind the simplified criteria are exposed and justified using a combination of rigorous results (Theorem 2.1 and Lemma 5.1), shallow amplitude asymptotics (Proposition 2.3), and computations of the spectrum. Consequences of the small-amplitude asymptotics and numerical computations are the first order corrections to the maximal growth rate and associated wavenumber (Corollary 2.4) and dependence of the critical Mach number on the soliton amplitude (Conclusion 3.5). Applying Conclusion 3.5 to the soliton trailing edge of oblique DSWs, we conclude that *subsonic oblique DSWs are always absolutely unstable, whereas supersonic oblique DSWs can be absolutely or convectively unstable* (Corollaries 4.2 and 4.3). In addition, the relationship between stationary DSWs (corner BVPs) and nonstationary DSWs (Riemann IVPs) is studied. In both cases, the DSWs are found to have the same downstream flow properties in the shallow and hypersonic regimes (Conclusion 4.4).

It is worth contrasting these results with oblique shock waves in classical gas dynamics. Supersonic classical shock fronts in gas dynamics are linearly *stable* when they satisfy the Lax entropy condition [23]. For the boundary value problem of supersonic flow past a sharp corner, the oblique shock is stable if and only if the downstream flow is supersonic [24, 25]. As far as we know, the distinction between absolute and convective instabilities in the subsonic case has not been elucidated. We note that recent experiments in another viscous medium (granular material) exhibit the stable excitation of oblique DSWs with both supersonic and subsonic downstream flow conditions [55].

Several questions and open problems related to this study are mentioned below.

The nonstationary oblique DSW consists of a slowly modulated elliptic function solution to NLS. How to study the stability or instability of this coherent structure is not immediately obvious given its expanding nature and asymptotic representation. The notion of instability we consider here is centered upon the properties of perturbations to the stationary trailing dark soliton edge. This is a natural criterion because the soliton trailing edge corresponds to the largest oscillation in the DSW;

hence nonlinear effects are strongest there. Another motivation for this choice comes from the numerical simulation of supersonic flow over a corner where the instability first appears along the trailing edge soliton. However, to gain a more complete understanding of DSW instabilities, one should develop an analysis of absolute and convective transverse instabilities of elliptic function solutions. This suggests the more general study of convective/absolute instability for systems with continuous bands of unstable modes. We are not aware of any previous work in this direction.

Careful computations of the spectrum suggest that Conjecture 2.2 is true. However, to the best of our knowledge, it has not been proved rigorously. It may be possible to do this by reducing the problem to an ODE, where Sturm–Liouville theory is applicable (cf. [56, 30]).

It would be interesting to extend the results obtained here for the KP-I equation to the KP-II equation. KP-II corresponds to negative (normal) dispersion, which arises in shallow water waves with small surface tension. In contrast to the KP-I line-solitons studied here, line-solitons of KP-II are linearly stable [28]. Since DSWs also occur in the KP-II equation (cf. [58]), this raises the question: Are DSWs in KP-II (and other systems with negative dispersion) stable?

Appendix A. Eigenvalue asymptotics. We seek the dispersion relation $\Omega(k; \nu)$ of (2.7) for unstable transverse perturbations to the shallow ($0 < \nu \ll 1$) dark line soliton (2.4). Rather than perform asymptotics directly on (2.7) it is convenient to consider the eigenvalue problem in fluid variables (1.2). The soliton solution (2.4) takes the form

$$(A.1a) \quad \rho(x, y, t) = \rho_s(\zeta) = 1 - \nu^2 \operatorname{sech}^2(\zeta),$$

$$(A.1b) \quad u(x, y, t) = u_s(\zeta) = \frac{-\kappa}{\sinh^2(\zeta) + \frac{\kappa^2}{\nu^2} \cosh^2(\zeta)},$$

$$(A.1c) \quad v(x, y, t) = 0, \quad \zeta = \nu(x - \kappa t).$$

Applying multiple scales to (1.3) leads to the KP-I equation for weakly nonlinear excitations of (1.1) to the uniform state $\rho \equiv 1$ (cf. [57]). The scalings involved motivate the following representation of weak transverse perturbations to the dark soliton (A.1)

$$\begin{aligned} \rho(x, y, t) &= \rho_s(\zeta) - \varepsilon f(\zeta) e^{i(p\eta - \Lambda\tau)}, \\ u(x, y, t) &= u_s(\zeta) - \varepsilon g(\zeta) e^{i(p\eta - \Lambda\tau)}, \\ v(x, y, t) &= \varepsilon \nu h(\zeta) e^{i(p\eta - \Lambda\tau)}, \\ \zeta &= \nu(x - \kappa t), \quad \eta = \nu^2 y, \quad \tau = \nu^3 t, \quad 0 < \varepsilon \ll 1. \end{aligned}$$

Inserting these expansions into (1.3) and (4.7c) while keeping only $\mathcal{O}(\varepsilon)$ terms gives

$$(A.2a) \quad -f u'_s - g \rho'_s + f' [\kappa - u_s] + \rho_s (-g' + i p \nu^2 h) = -i \nu^2 \Lambda f,$$

$$\begin{aligned} & -\frac{\nu^2 \rho'_s}{\rho_s^3} (3f' \rho'_s + 4f \rho''_s) + \frac{3\nu^2 f \rho_s'^3}{\rho_s^4} + 4g u'_s \\ & + \frac{\nu^2}{\rho_s^2} [\rho'_s (2f'' - p^2 \nu^2 f) + 2f' \rho''_s(\zeta) + f \rho_s'''] \\ (A.2b) \quad & + 4[f' + g' (u_s - \kappa)] + \frac{1}{\rho_s} (p^2 \nu^4 f' - \nu^2 f''') = 4i \nu^2 \Lambda g, \\ (A.2c) \quad & h' = -i p g. \end{aligned}$$

This is an eigenvalue problem parameterized by p and ν for the eigenvalue $\Lambda = \Lambda(p; \nu)$ and eigenfunction $[f, g, h]^T$.

Assuming $p \notin \{0, \pm p_{\text{cutoff}}\}$ where $p_{\text{cutoff}} = k_{\text{cutoff}}/\nu^2$ so that the eigenvalue of interest is simple, we expand² the coefficient functions ρ_s and u_s , the parameter $\kappa = \sqrt{1 - \nu^2}$, the eigenfunction $[f, g, h]^T$, and the eigenvalue Λ in powers of ν^2 :

$$\begin{aligned} (A.3) \quad & f = f_0 + \nu^2 f_1 + \nu^4 f_2 + \cdots, \\ & g = f_0 + \nu^2 g_1 + \nu^4 g_2 + \cdots, \\ & h = -ip \int (f_0 + \nu^2 g_1 + \nu^4 g_2 + \cdots) d\zeta, \\ & \Lambda(p; \nu) = \Lambda_0(p) + \nu^2 \Lambda_1(p) + \cdots. \end{aligned}$$

Then, (A.2c) is automatically satisfied to all orders so we only consider equations (A.2a) and (A.2b) which expand, respectively, as

$$\begin{aligned} (A.4a) \quad & \left\{ f_1' - g_1' + \left[\left(2\text{sech}^2(\zeta) - \frac{1}{2} \right) f_0 \right]' + i\Lambda_0 f_0 + p^2 \int f_0 d\zeta \right\} \\ & + \nu^2 \left\{ f_2' - g_2' - \frac{1}{2} \text{sech}^2(\zeta) \left(-2(f_1' + g_1') + f_0' + 2p^2 \int f_0 d\zeta \right) \right. \\ & \quad - \frac{1}{8} f_0' - \frac{1}{2} f_1' \text{sech}^4(\zeta) f_0' + \tanh(\zeta) \text{sech}^2(\zeta) (f_0 - 2(f_1 + g_1)) \\ & \quad \left. + i\Lambda_1 f_0 + i\Lambda_0 f_1 - 4f_0 \tanh(\zeta) \text{sech}^4(\zeta) + p^2 \int g_1 d\zeta \right\} = \mathcal{O}(\nu^4), \end{aligned}$$

$$\begin{aligned} (A.4b) \quad & \left\{ g_1' - f_1' + \left[\left(\text{sech}^2(\zeta) - \frac{1}{2} \right) f_0 \right]' + \frac{1}{4} f_0''' + i\Lambda_0 f_0 \right\} \\ & + \frac{\nu^2}{8} \left\{ 8g_2' - 8f_2' + 8f_0 \text{sech}^2(\zeta) \tanh(\zeta) (2\text{sech}^2(\zeta) - 1) \right. \\ & \quad + 2\text{sech}^2(\zeta) [-4 \tanh(\zeta) (f_0'' + 2g_1) + f_0''' + 4g_1'] \\ & \quad + 2\text{sech}^2(\zeta) (6 - 8\text{sech}^2(\zeta)) f_0' - (2p^2 + 1) f_0' \\ & \quad \left. + 2f_1''' - 4g_1' + 8i\Lambda_1 f_0 + 8i\Lambda_0 g_1 \right\} = \mathcal{O}(\nu^4). \end{aligned}$$

A.1. KP eigenvalue problem. Adding (A.4a) to (A.4b) gives

$$\frac{1}{4} \left[f_0''' - 4[(1 - 3\text{sech}^2(\zeta))f_0]' + 8i\Lambda_0 f_0 + 4p^2 \int f_0 d\zeta \right] = \mathcal{O}(\nu^2).$$

Differentiating and keeping only leading order terms gives

$$\mathcal{L}f_0 \doteq f_0'''' - 4[(1 - 3\text{sech}^2(\zeta))f_0]'' + 8i\Lambda_0 f_0' + 4p^2 f_0 = 0.$$

²The two limits, linearization about the soliton and expanding in ν , are not interchangeable.

This is the KP eigenvalue problem studied in [28]. The unstable portion of the spectrum includes one eigenpair,

$$f_0(\zeta; p) = \frac{d^2}{d\zeta^2} \left\{ e^{(1+\sqrt{1-2p/\sqrt{3}})\zeta} \left[2 - 2p/\sqrt{3} + 2\sqrt{1-2p/\sqrt{3}} \right] [1 - \tanh(\zeta)] \right\},$$

$$\Lambda_0(p) = -i\frac{p}{3}\sqrt{3-2\sqrt{3}p}, \quad 0 < p < \frac{\sqrt{3}}{2} \sim p_{\text{cutoff}}, \quad 0 < \nu \ll 1.$$

This eigenvalue is continued onto the positive real line by the eigenpair

$$f_0(\zeta; p) = \frac{d^2}{d\zeta^2} \left\{ e^{(1-i\sqrt{2p/\sqrt{3}-1})\zeta} \left[2 - 2p/\sqrt{3} + 2i\sqrt{2p/\sqrt{3}-1} \right] [1 - \tanh(\zeta)] \right\},$$

$$\Lambda_0(p) = \frac{p}{3}\sqrt{2\sqrt{3}p-3}, \quad p > \frac{\sqrt{3}}{2} \sim p_{\text{cutoff}}, \quad 0 < \nu \ll 1.$$

A.2. Perturbed KP eigenvalue problem. Below we determine the correction $\Lambda_1(p)$. f_1 is determined in terms of g_1 by subtracting (A.4a) from (A.4b) to obtain

$$2f_1' - 2g_1' - \frac{1}{4}f_0''' + [\text{sech}^2(\zeta)f_0]' + p^2 \int f_0 d\zeta = \mathcal{O}(\nu^2),$$

so that

$$(A.5) \quad f_1 = g_1 + \frac{1}{8}f_0'' - \frac{1}{2}\text{sech}^2(\zeta)f_0 - \frac{p^2}{2} \int \int f_0 d\zeta + \mathcal{O}(\nu^2)$$

$$\doteq g_1 + \tilde{f} + \mathcal{O}(\nu^2), \quad \tilde{f} = \frac{1}{8}f_0'' - \frac{1}{2}\text{sech}^2(\zeta)f_0 - \frac{p^2}{2} \int \int f_0 d\zeta.$$

Using (A.5) in (A.4a) and (A.4b), adding the two equations together, and differentiating, the $\mathcal{O}(\nu^2)$ terms equate to

$$\begin{aligned} \mathcal{L}g_1 = & -\text{sech}^2(\zeta) \left[4 \left(3f_0'' - p^2 f_0 + \tilde{f}'' + 4\tilde{f} \right) + f_0'''' \right] \\ & + 2 \tanh(\zeta) \text{sech}^2(\zeta) \left(4f_0' + 3f_0''' - 4p^2 \int f_0 d\zeta + 8\tilde{f}' \right) \\ & + 8\text{sech}^4(\zeta) \left(2f_0'' - 4f_0 + 3\tilde{f} \right) + p^2 f_0'' - 4i\Lambda_0 \tilde{f}' \\ & - 8 \tanh(\zeta) \text{sech}^4(\zeta) f_0' + f_0''(\zeta) - \tilde{f}'''' + 40f_0 \text{sech}^6(\zeta) \\ & + 2\tilde{f}'' - 8i\Lambda_1 f_0' \\ \doteq & G(\zeta; p) - 8i\Lambda_1 f_0'. \end{aligned}$$

Solvability then determines Λ_1

$$(A.6) \quad \Lambda_1(p) = -i \frac{\int_{-\infty}^{\infty} G(\zeta; p) h^*(\zeta; p) d\zeta}{8 \int_{-\infty}^{\infty} f_0'(\zeta; p) h^*(\zeta; p) d\zeta},$$

where $h(\zeta; p)$ is the homogeneous solution of the adjoint problem

$$\mathcal{L}^\dagger h = h'''' - 4(1 - 3\text{sech}^2\zeta)h'' + 8i\Lambda_0^* h' + 4p^2 h = 0.$$

Since Λ_0 is either purely real or purely imaginary, the solution of the adjoint problem is

$$h(\zeta; p) = \begin{cases} f_0^*(\zeta; p), & p < \frac{\sqrt{3}}{2}, \\ f_0(\zeta; p), & p > \frac{\sqrt{3}}{2}. \end{cases}$$

The integrals in (A.6) can be calculated explicitly:

$$\Lambda_1(p) = \frac{p^2 (\sqrt{3} - p)}{6\sqrt{2\sqrt{3}p - 3}}.$$

For the asymptotic expansion in (A.3) to be valid, we require $\Lambda_0(p) \gg \nu^2 \Lambda_1(p)$. This puts a restriction on the values of p where the expansion is valid:

$$p_{\text{cutoff}} < p \ll \frac{1}{\nu^2} \quad \text{or} \quad 0 < p < p_{\text{cutoff}}, \quad 0 < \nu \ll 1.$$

Then, the unscaled eigenvalue $\Omega(k; \nu)$ in (2.7) has the asymptotic expansion

$$\begin{aligned} \Omega(k; \nu) &\sim \nu^3 \Lambda_0(k/\nu^2) + \nu^5 \Lambda_1(k/\nu^2), \\ k &< k_{\text{cutoff}}(\nu), \quad k_{\text{cutoff}}(\nu) < k = \mathcal{O}(\nu^2) \ll 1, \quad 0 < \nu \ll 1, \end{aligned}$$

which is given in (2.13).

Appendix B. Theorem 2.1. In [30] it was proved that L_0 has exactly one negative eigenvalue which was determined explicitly in [8] $(L_0 + k_{\text{cutoff}}^2/2)\mathbf{f} = 0$. In addition, it was proved in [56] from general considerations of linear operators of the form JL , where J is skew-symmetric and L is symmetric, that the number of eigenvalues of JL with a positive real part is at most the number of negative eigenvalues of L . The latter decomposition applies to (2.8), where $L = L_0 + k^2/2$ is symmetric for $k \in \mathbb{R}$ and J is skew-symmetric.

Combining these results, for $0 < |k| < k_{\text{cutoff}}$, $k \in \mathbb{R}$, L has one negative eigenvalue and therefore JL has at most one eigenvalue with a positive real part. By the instability of the dark soliton, proven in [30], JL has exactly one eigenvalue with positive real part. There is also exactly one eigenvalue with negative real part via the following lemma.

LEMMA B1. *For $k \in \mathbb{R}$, the eigenvalues of JL come in pairs of opposite sign.*

Proof. For any $k \in \mathbb{R}$,

$$(B.1) \quad JL = -R\sigma_3 L J R \sigma_3.$$

Let $JL\mathbf{f} = \Gamma\mathbf{f}$. Using (B.1) and one of the Pauli matrices (5.1) gives

$$JLR\sigma_3\mathbf{f} = -\Gamma R\sigma_3\mathbf{f}.$$

It follows that $(-\Gamma, R\sigma_3\mathbf{f})$ is also an eigenpair for JL . \square

On the other hand, for $|k| > k_{\text{cutoff}}$, $k \in \mathbb{R}$, L has no negative eigenvalues and therefore, by Lemma B1, JL has only purely imaginary eigenvalues. We find numerically and asymptotically in the shallow regime only two discrete, simple eigenvalues for $k \in \mathbb{C} \setminus \{0, \pm k_{\text{cutoff}}\}$.

Appendix C. Proof of Lemma 5.1. We make use of the following identity:

$$(C.1) \quad JL_0 = R\sigma_1 L_0 J R \sigma_1.$$

For any $k \in \mathbb{C}$, consider (Ω_0, \mathbf{f}_0) an eigenpair for (2.7) satisfying

$$(C.2) \quad \left[J \left(L_0 + \frac{1}{2}k^2 \right) + i\Omega_0 \right] \mathbf{f}_0 = 0.$$

Since Ω_0 is a simple eigenvalue, it follows that

$$\dim \left(\ker \left\{ \left[JL_0 + \frac{1}{2}k^2 J + i\Omega_0 \right]^\dagger \right\} \right) = 1.$$

Therefore, it remains to verify that $R\sigma_1 \mathbf{f}_0^*$ is in the nullspace of $[JL_0 + \frac{1}{2}k^2 J + i\Omega_0]^\dagger$. We take the complex conjugate of (C.2) and apply the decomposition (C.1) to obtain

$$\left[-R\sigma_1 L_0 J R\sigma_1 + \frac{1}{2}k^{*2} J - i\Omega_0^* \right] \mathbf{f}_0^* = 0.$$

Applying $R\sigma_1$ yields

$$- \left[L_0 J + \frac{1}{2}k^{*2} J + i\Omega_0^* \right] R\sigma_1 \mathbf{f}_0^* = 0,$$

which is precisely the adjoint equation to (C.2). Therefore, we have

$$\ker \left\{ \left[J \left(L_0 + \frac{1}{2}k^2 \right) + i\Omega_0 \right]^\dagger \right\} = \text{span}\{R\sigma_1 \mathbf{f}_0^*\}, \quad k \in \mathbb{C}.$$

By similar arguments with $JL_0 = -\sigma_2 L_0 J \sigma_2$, one can show that $\sigma_2 \mathbf{f}_0 \propto R\sigma_1 \mathbf{f}_0^*$ and hence spans the kernel of $[JL_0 + \frac{1}{2}k^2 J + i\Omega_0]^\dagger$ when $k, \Omega_0 \in \mathbb{R}$. We use this null eigenfunction in our numerical computations whenever $k \in (k_{\text{cutoff}}, \infty)$.

Acknowledgments. The authors thank Mark Ablowitz for inspiring remarks. The authors also thank Anatoly Kamchatnov for constructive discussions and sharing his recent manuscript [49].

REFERENCES

- [1] Y. S. KIVSHAR AND D. E. PELINOVSKY, *Self-focusing and transverse instabilities of solitary waves*, Phys. Rep., 331 (2000), pp. 117–195.
- [2] D. J. FRANTZESKAKIS, *Dark solitons in atomic Bose-Einstein condensates: From theory to experiments*, J. Phys. A, 43 (2010), 213001.
- [3] T. J. BRIDGES, *Transverse instability of solitary-wave states of the water-wave problem*, J. Fluid Mech., 439 (2001), pp. 255–278.
- [4] B. AKERS AND P. A. MILEWSKI, *Dynamics of three-dimensional gravity-capillary solitary waves in deep water*, SIAM J. Appl. Math., 70 (2010), pp. 2390–2408.
- [5] B. B. KADOMTSEV AND V. I. PETVIASHVILI, *On the stability of solitary waves in weakly dispersing media*, Sov. Phys. Dokl., 15 (1970), pp. 539–541.
- [6] V. E. ZAKHAROV, *Instability and nonlinear oscillations of solitons*, JETP Lett., 22 (1975), pp. 172–173.
- [7] V. E. ZAKHAROV AND A. M. RUBENCHIK, *Instability of waveguides and solitons in nonlinear media*, Sov. Phys. JETP, 38 (1974), pp. 494–500.
- [8] E. A. KUZNETSOV AND K. TURITSYN, *Instability and collapse of solitons in media with a defocusing nonlinearity*, Sov. Phys. JETP, 67 (1981), pp. 1583–1586.
- [9] G. A. EL, A. GAMMAL, AND A. M. KAMCHATNOV, *Oblique dark solitons in supersonic flow of a Bose-Einstein condensate*, Phys. Rev. Lett., 97 (2006), 180405.
- [10] Y. G. GLADUSH, A. M. KAMCHATNOV, Z. SHI, P. G. KEVREKIDIS, D. J. FRANTZESKAKIS, AND B. A. MALOMED, *Wave patterns generated by a supersonic moving body in a binary Bose-Einstein condensate*, Phys. Rev. A, 79 (2009), 033623.
- [11] A. M. KAMCHATNOV AND L. P. PITAEVSKIĬ, *Stabilization of solitons generated by a supersonic flow of Bose-Einstein condensate past an obstacle*, Phys. Rev. Lett., 100 (2008), 160402.
- [12] P. A. STURROCK, *Kinematics of growing waves*, Phys. Rev., 112 (1958), pp. 1488–1503.

- [13] R. G. BRIGGS, *Electron-Stream Interaction with Plasmas*, MIT Press, Cambridge, MA, 1964.
- [14] C. M. DAFERMOS, *Hyperbolic Conservation Laws in Continuum Physics*, 3rd ed., Springer-Verlag, New York, 2009.
- [15] M. A. HOEFER AND M. J. ABLOWITZ, *Dispersive shock waves*, Scholarpedia, 4 (2009), p. 5562.
- [16] Z. DUTTON, M. BUDDE, C. SLOWE, AND L. V. HAU, *Observation of quantum shock waves created with ultra-compressed slow light pulses in a Bose-Einstein condensate*, Science, 293 (2001), p. 663.
- [17] M. A. HOEFER, M. J. ABLOWITZ, I. CODDINGTON, E. A. CORNELL, P. ENGELS, AND V. SCHWEIKHARD, *Dispersive and classical shock waves in Bose-Einstein condensates and gas dynamics*, Phys. Rev. A, 74 (2006), 023623.
- [18] R. MEPPELINK, S. B. KOLLER, J. M. VOGELS, P. VAN DER STRATEN, E. D. VAN OOIJEN, N. R. HECKENBERG, H. RUBINSZTEIN-DUNLOP, S. A. HAINE, AND M. J. DAVIS, *Observation of shock waves in a large Bose-Einstein condensate*, Phys. Rev. A, 80 (2009), 043606.
- [19] W. WAN, S. JIA, AND J. W. FLEISCHER, *Dispersive superfluid-like shock waves in nonlinear optics*, Nat. Phys., 3 (2007), pp. 46–51.
- [20] C. CONTI, A. FRATALOCCHI, M. PECCANTI, G. RUOCCO, AND S. TRILLO, *Observation of a gradient catastrophe generating solitons*, Phys. Rev. Lett., 102 (2009), 083902.
- [21] A. ARMAROLI, S. TRILLO, AND A. FRATALOCCHI, *Suppression of transverse instabilities of dark solitons and their dispersive shock waves*, Phys. Rev. A, 80 (2009), 053803.
- [22] M. A. HOEFER AND B. ILAN, *Theory of two-dimensional oblique dispersive shock waves in supersonic flow of a superfluid*, Phys. Rev. A, 80 (2009), 061601(R).
- [23] A. MAJDA, *The stability of multidimensional shock fronts*, Mem. Amer. Math. Soc., 275 (1983).
- [24] D. LI, *Analysis on linear stability of oblique shock waves in steady supersonic flow*, J. Differential Equations, 207 (2004), pp. 195–225.
- [25] D. L. TKACHEV AND A. M. BLOKHIN, *Courant-Friedrich’s hypothesis and stability of the weak shock*, Proc. Sympos. Appl. Math., 67 (2009), p. 959.
- [26] K. ZUMBRUN, H. K. JENSEN, AND G. LYG, *Stability of large-amplitude shock waves of compressible Navier-Stokes equations*, in Handbook of Mathematical Fluid Dynamics, vol. 3, S. Friedlander and D. Serre, eds., Elsevier, Amsterdam, 2005, pp. 311–533.
- [27] R. COURANT AND K. O. FRIEDRICHS, *Supersonic Flow and Shock Waves*, Springer-Verlag, Berlin, 1948.
- [28] J. C. ALEXANDER, R. L. PEGO, AND R. L. SACHS, *On the transverse instability of solitary waves in the Kadomtsev-Petviashvili equation*, Phys. Lett. A, 226 (1997), pp. 187–192.
- [29] D. PELINOVSKY, Y. STEPANYANTS, AND Y. KIVSHAR, *Self-focusing of plane dark solitons in nonlinear defocusing media*, Phys. Rev. E, 51 (1995), pp. 5016–5026.
- [30] F. ROUSSET AND N. TZVETKOV, *A simple criterion of transverse linear instability for solitary waves*, Math. Res. Lett., 17 (2010), pp. 157–169.
- [31] L. P. PITAEVSKIĬ AND E. LIFSHITZ, *Physical Kinetics*, Course of Theoretical Physics 10, Pergamon Press, Oxford, UK, 1981, pp. 268–273.
- [32] E. INFELD AND G. ROWLANDS, *Nonlinear Waves, Solitons and Chaos*, Cambridge University Press, Cambridge, UK, 1990.
- [33] P. J. SCHMID AND D. S. HENNINGSON, *Stability and Transition in Shear Flows*, Appl. Math. Sci. 142, Springer-Verlag, New York, 2000.
- [34] A. BERS, *Space-Time Evolution of Plasma Instabilities—Absolute and Convective*, vol. 1, Elsevier, Amsterdam, 1983, pp. 451–517.
- [35] P. HUERRE AND P. A. MONKEWITZ, *Absolute and convective instabilities in free shear layers*, J. Fluid Mech., 159 (1985), pp. 151–168.
- [36] L. BREVDO AND T. J. BRIDGES, *Absolute and convective instabilities of spatially periodic flows*, Phil. Trans. Roy. Soc. Lond. A, 354 (1996), pp. 1027–1064.
- [37] P. D. MILLER, *Applied Asymptotic Analysis*, AMS Publications, Providence, RI, 2006.
- [38] V. A. MIRONOV, A. I. SMIRNOV, AND L. A. SMIRNOV, *Structure of vortex shedding past potential barriers moving in a Bose-Einstein condensate*, JETP, 110 (2010), pp. 877–889.
- [39] G. A. EL, A. M. KAMCHATNOV, V. V. KHODOROVSKIĬ, E. S. ANNIBALE, AND A. GAMMAL, *Two-dimensional supersonic nonlinear Schrödinger equation flow past an extended obstacle*, Phys. Rev. E, 80 (2009), 046317.
- [40] G. B. WHITHAM, *Non-linear dispersive waves*, Proc. Roy. Soc. Ser. A, 283 (1965), pp. 238–261.
- [41] A. V. GUREVICH AND L. P. PITAEVSKIĬ, *Nonstationary structure of a collisionless shock wave*, Sov. Phys. JETP, 38 (1974), pp. 291–297.
- [42] A. V. GUREVICH AND A. L. KRYLOV, *Dissipationless shock waves in media with positive dispersion*, Sov. Phys. JETP, 65 (1987), pp. 944–953.
- [43] G. A. EL, R. H. J. GRIMSHAW, AND N. F. SMYTH, *Unsteady undular bores in fully nonlinear shallow-water theory*, Phys. Fluids, 18 (2006), 027104.

- [44] G. A. EL, A. GAMMAL, E. G. KHAMIS, R. A. KRAENKEL, AND A. M. KAMCHATNOV, *Theory of optical dispersive shock waves in photorefractive media*, Phys. Rev. A, 76 (2007), 053813.
- [45] G. A. EL, *Resolution of a shock in hyperbolic systems modified by weak dispersion*, Chaos, 15 (2005), 037103.
- [46] A. V. GUREVICH, A. L. KRYLOV, V. V. KHODOROVSKII, AND G. A. EL, *Supersonic flow past bodies in dispersive hydrodynamics*, Sov. Phys. JETP, 81 (1995), pp. 87–96.
- [47] A. V. GUREVICH, A. L. KRYLOV, V. V. KHODOROVSKII, AND G. A. EL, *Supersonic flow past finite-length bodies in dispersive hydrodynamics*, Sov. Phys. JETP, 82 (1996), pp. 709–718.
- [48] G. A. EL AND A. M. KAMCHATNOV, *Spatial dispersive shock waves generated in supersonic flow of Bose-Einstein condensate past slender body*, Phys. Rev. A, 350 (2006), pp. 192–196.
- [49] A. M. KAMCHATNOV AND S. V. KORNEEV, *Condition for convective instability of dark solitons*, Phys. Lett. A, 375 (2011), pp. 2577–2580.
- [50] W. D. HAYES AND R. F. PROBSTEN, *Hypersonic Inviscid Flow*, Dover, New York, 2004.
- [51] M. A. HOEFER, M. J. ABLOWITZ, AND P. ENGELS, *Piston dispersive shock wave problem*, Phys. Rev. Lett., 100 (2008), 084504.
- [52] A. KAMCHATNOV AND S. KORNEEV, *Flow of a Bose-Einstein condensate in a quasi-one-dimensional channel under the action of a piston*, JETP, 110 (2010), pp. 170–182.
- [53] G. KEETELS, U. D’ORTONA, W. KRAMER, H. CLERCX, K. SCHNEIDER, AND G. VAN HEIJST, *Fourier spectral and wavelet solvers for the incompressible Navier-Stokes equations with volume-penalization: Convergence of a dipole-wall collision*, J. Comput. Phys., 227 (2007), pp. 919–945.
- [54] M. J. ABLOWITZ AND Z. H. MUSSLIMANI, *Spectral renormalization method for computing self-localized solutions to nonlinear systems*, Opt. Lett., 30 (2005), pp. 2140–2142.
- [55] J. M. N. T. GRAY, AND X. CUI, *Weak, strong and detached oblique shocks in gravity-driven granular free-surface flows*, J. Fluid Mech., 579 (2007), pp. 113–136.
- [56] R. L. PEGO AND M. I. WEINSTEIN, *Eigenvalues, and instabilities of solitary waves*, Phil. Trans. Roy. Soc. London Ser. A, 340 (1992), pp. 47–94.
- [57] V. ZAKHAROV AND E. KUZNETSOV, *Multi-scale expansions in the theory of systems integrable by the inverse scattering transform*, Phys. D, 18 (1986), pp. 455–463.
- [58] C. KLEIN, C. SPARBER, AND P. MARKOWICH, *Numerical study of oscillatory regimes in the Kadomtsev–Petviashvili equation*, J. Nonlinear Sci., 17 (2007), pp. 429–470.